Marisa Raquel Martins de Brito Ferreira

Licenciatura em Bioquímica

Characterization and interaction studies of triheme cytochromes from *Geobacter*: a contribution to the elucidation of extracellular electron transfer pathways

Dissertação para obtenção do Grau de Mestre em Bioquímica

Orientador: Prof. Doutor Carlos A. Salgueiro,
Professor Auxiliar com Agregação
Faculdade de Ciências e Tecnologia, Universidade Nova de Lisboa

Júri:
Arguente: Prof. Doutor Eurico José da Silva Cabrita
Vogal: Prof. Doutor Carlos A. Salgueiro

FACULDADE DE CIÊNCIAS E TECNOLOGIA
UNIVERSIDADE NOVA DE LISBOA

Outubro 2016

Universidade Nova de Lisboa

Marisa Raquel Martins de Brito Ferreira

Licenciatura em Bioquímica

Characterization and interaction studies of triheme cytochromes from *Geobacter*: a contribution to the elucidation of extracellular electron transfer pathways

Dissertação para obtenção do Grau de Mestre em Bioquímica

Orientador: Prof. Doutor Carlos A. Salgueiro, Professor Auxiliar com Agregação, Faculdade de Ciências e Tecnologia, Universidade Nova de Lisboa

Outubro 2016

Characterization and interaction studies of triheme cytochromes from *Geobacter*: a contribution to the elucidation of extracellular electron transfer pathways

The results obtained under the scope of this thesis are under review in the Dalton Transactions Journal [1]. Additionally, the results were presented as oral communication[2] in the national congress MicroBiotec 2015 and were already accepted for oral communication[3] in the XIX National Congress of Biochemistry SPB 2016.

[1] Marisa R. Ferreira, Joana M. Dantas and Carlos A. Salgueiro, Molecular interactions between *Geobacter sulfurreducens* triheme cytochromes and the electron acceptor Fe(III) citrate studied by NMR, 2016

[2] Marisa R. Ferreira, Joana M. Dantas, Teresa Catarino, David L. Turner and Carlos A. Salgueiro, Interactions studies between a redox active component of humic substances and a family of cytochromes from *Geobacter sulfurreducens* involved in extracellular electron transfer, VI MicroBiotec 2015

[3] Marisa R. Ferreira, Joana M. Dantas and Carlos A. Salgueiro, First evidence for molecular interactions between *Geobacter sulfurreducens* triheme cytochromes and the terminal electron acceptor Fe(III) citrate, XIX National Congress of Biochemistry SPB 2016

AGRADECIMENTOS

Em primeiro lugar, quero agradecer ao Prof. Doutor Carlos Salgueiro, por todo o apoio, disponibilidade, amizade e ensinamentos que me proporcionou ao longo deste trabalho. Agradeço também a sua dedicação, por ter acreditado nas minhas capacidades, pelas longas conversas e por toda a motivação que sempre me deu quando mais precisei.

Quero também agradecer à Joana Dantas pela disponibilidade e ajuda, por partilhar comigo os seus conhecimentos e pela boa disposição e gargalhadas diárias.

Aos meus colegas de laboratório, Ana Fernandes, Marta Silva, Liliana Teixeira, Tomás Fernandes e Tiago Nunes pelo bom ambiente e dinamismo proporcionado e que sempre se mostraram prontos a ajudar.

Um especial obrigado às minhas febras, Carina Figueiredo, Patrícia Reis, Cindy Soares, Cindy Oliveira e Filipa Trovão por todo o apoio que sempre me deram ao longo não só deste trabalho, mas nos últimos 5 anos. Nada seria o mesmo sem a vossa presença. Obrigada pelas conversas, pelos almoços, jantares, festas, choros, desabafos, abraços, os bons e maus momentos, tudo. Sem dúvida que vos levarei sempre comigo.

À Helena Portela, Décio Resendes e Filipa Belchior por todos os momentos e motivação que sempre me deram ao longo desta etapa da minha vida. Obrigada por sempre terem acreditado em mim.

Por fim gostaria de agradecer à minha mãe pelo apoio, compreensão, paciência e por sempre ter acreditado nas minhas capacidades. Sem ti nada disto seria alguma vez possível.

O trabalho desenvolvido no âmbito desta tese foi financiado pelos seguintes projetos: PTDC/BBB-BQB/3554/2014 e UID/Multi/04378/2013 da Fundação para a Ciência e a Tecnologia, Portugal. Os espectrómetros de NMR fazem parte da *National NMR Facility*, financiada pela Fundação para a Ciência e a Tecnologia (RECI/BBB-BQB/0230/2012).

ABSTRACT

Geobacter species are frequently the most abundant Fe(III)-reducing microorganism in soils and sediments. They can also reduce other metals in the same type of environments and, in addition, make electrical connections with electrodes to produce electricity from waste organic matter or to drive anaerobic process with electrical energy. Proteomic and genetic studies have identified several multiheme cytochromes as essential for Fe(III) reduction. From all the cytochromes that were shown to be involved in the reduction of Fe(III), the best characterized to date are five periplasmic triheme cytochromes from *Geobacter sulfurreducens,* which constitute the so-called PpcA-family. The members of this family are designated PpcA, PpcB, PpcC, PpcD, PpcE. A similar family was found in *Geobacter metallireducens* (PpcA, PpcB, PpcC, PpcE and PpcF) but none of these proteins was characterized to date. When compared to the other homologs found in *G. sulfurreducens*, PpcF differs the most and for this reason was targeted in the present work. To characterize this cytochrome, PpcF was firstly expressed and purified. The yield obtained was approximately 1 mg/L of cell culture. The molecular mass of the protein was confirmed by mass spectroscopy (9737.13 Da). The molar extinction coefficient was determined (87.4 $mM^{-1}cm^{-1}$). The UV-visible spectral characteristics of PpcF are consistent with low-spin heme groups with His-His axial coordination, a feature that was further confirmed by Nuclear Magnetic Resonance spectroscopy. The assignment of the heme substituent signals of PpcF in both reduced and oxidized states together with the analysis of their NOE connectivities showed that the heme core structure is similar to those of the PpcA family cytochromes in *G. sulfurreducens*. The reduction potentials of PpcF were determined at pH 7 and 8 (-56 mV and – 64 mV *versus* the standard hydrogen electrode, respectively). Lastly 2D-^{1}H NMR exchange spectroscopy was used to determine the order of oxidation of the heme groups in PpcF: IV-I-III.

In the second part of this thesis it was analyzed the possible molecular interaction between cytochromes PpcA, PpcB and PpcE from *G. sulfurreducens* and Fe(III) citrate. This molecule can be utilized as terminal electron acceptor by this bacterium and PpcA, PpcB and PpcE were shown to be crucial in this electron transfer pathway. For these purpose isotopic ^{15}N-labeled cytochromes were expressed and purified. NMR spectroscopy enabled us to assign the protein NH backbone and heme methyl proton signals, as well as to probe the interaction regions between each cytochrome and

Fe(III) citrate. The chemical shift perturbation studies showed that in all cytochromes the interaction region is located in the vicinity of heme IV.

RESUMO

Os microrganismos redutores de Fe(III) da espécie *Geobacter* são frequentemente os mais abundantes em solos e sedimentos. Estes podem também reduzir outros metais no mesmo meio de crescimento sendo ainda capazes de transferir eletrões para superfícies de elétrodos com concomitante produção de corrente elétrica a partir de matéria orgânica. Estudos genéticos e proteómicos mostraram que alguns citocromos multihémicos são fundamentais nas cadeias respiratórias envolvidas na redução de Fe(III). Destes, os melhor caracterizados até à data são cinco citocromos trihémicos periplasmáticos de *Geobacter sulfurreducens*. Estes citocromos são designados PpcA, PpcB, PpcC, PpcD e PpcE. Uma família semelhante foi encontrada em *Geobacter metallireducens* (PpcA, PpcB, PpcC, PpcE e PpcF). Nenhum destes citocromos foi caraterizado até ao momento. PpcF é o citocromo que mais difere em homologia quando comparado com os membros da família PpcA em *G. sulfurreducens* e por essa razão foi escolhido para ser estudado neste trabalho. De forma a caracterizar este citocromo, a proteína foi primeiramente expressa e purificada. O rendimento desta expressão foi de aproximadamente 1 mg por litro de cultura celular. A massa molecular desta proteína foi confirmada por espectrometria de massa (9737.13 Da). O coeficiente de extinção molar foi determinado (87.4 $mM^{-1}cm^{-1}$). O espectro UV-visível deste citocromo apresenta as características espectrais típicas de grupos hemo de baixo *spin* com coordenação axial His-His, uma particularidade que foi confirmada por espectroscopia de Ressonância Magnética Nuclear. A atribuição dos sinais dos substituintes hémicos do PpcF no estado reduzido e oxidado, em conjunto com a análise das suas conectividades NOE, mostrou que a disposição espacial dos grupos hemo é semelhante à dos citocromos da família PpcA de *G. sulfurreducens*. Os potenciais de redução do PpcF foram determinados a pH 7 e 8 (-56 mV e -64 mV *versus* o elétrodo padrão de hidrogénio, respetivamente). Por último, experiências de RMN de permuta química foram efetuadas para determinar a ordem de oxidação dos grupos hemo nesta proteína: IV-I-III.

Na segunda parte desta tese foi analisada a possível interação entre os citocromos PpcA, PpcB e PpcE de *G. sulfurreducens* e o citrato de Fe(III). Esta molécula pode ser utilizada como aceitador final de eletrões nesta bactéria, tendo sido demostrado que os citocromos PpcA, PpcB e PpcE desempenham um papel crucial nesta via respiratória. Para este propósito os referidos citocromos foram expressos e purificados marcados isotopicamente em ^{15}N. A espectroscopia de RMN permitiu atribuir os sinais NH da cadeia principal da proteína e dos protões dos grupos metilo hémicos. Em conjunto, as perturbações observadas nestes sinais permitiram determinar as regiões de interação entre cada citocromo e o citrato de Fe(III). O estudo das perturbações nos desvios químicos demonstrou que em todos os citocromos a região de interação está localizada na vizinhança do hemo IV.

LIST OF CONTENTS

LIST OF FIGURES

LIST OF TABLES

LIST OF APPENDIX

LIST OF ABBREVIATIONS AND SYMBOLS

1D – One dimensional

2D – Two dimensional

2xYT – 2x yeast extract - tryptone medium

3D – Three dimensional

^{13}C – Carbon proton

^{15}N – Nitrogen proton

Å - Angstroms

AMP – Ampicillin

BCA – Bicinchoninic acid assay

C_α – Alpha carbon

C_β – Beta carbon

CLO – Chloramphenicol

D_2O – Deuterium oxide

Da – Dalton

E_{app} – Apparent midpoint potential value

EDTA – Ethylenediamine tetra-acetic acid

EXSY – Exchange spectroscopy

F – Faraday's constant

FID – Free induction decay

g - grams

g – g-force

Gm – Geobacter metallireducens

Gs – Geobacter sulfurreducens

HMQC – Heteronuclear multi-quantum correlation

HSQC – Heteronuclear single-quantum coherence

Hz - Hertz

IPTG – Isopropyl β-D-1-thiogalactopyranoside

IUPAC-IUB – International union of pure and applied chemistry and international union of biochemistry

K – Kelvin

L – Liter(s)

M - Molar

min – Minute(s)

ms – Milliseconds

mV – Millivolts

MW – Molecular weight

NaPi – Sodium phosphate buffer

NH – Amine hydrogen proton

nm - Nanometers

NMR – Nuclear magnetic resonance spectroscopy

NOE – Nuclear Overhauser effect

NOESY - Nuclear Overhauser effect spectroscopy

OD_{600} – Optical density at 600 nm

PDB – Protein data bank

pI – Isoelectric point

Ppc(x) – Periplasmic cytochrome (x)

ppm – Parts per million

R – Gas constant

rpm – rotation per minute

S – Spin angular momentum

SDS-PAGE – Sodium dodecyl sulfate polyacrylamide gel electrophoresis

SHE – Standard Hydrogen Electrode

TCI – Triple-resonance cryoprobe

TOCSY – Total correlation spectroscopy

Tris – Tris(hydroxymethyl)aminomethane

UV-visible – Ultraviolet-visible

δ – Chemical shift

°C – Degrees Celsius

ε_{552} – Extinction absorption coefficient at 552 nm

Chapter 1: Introduction

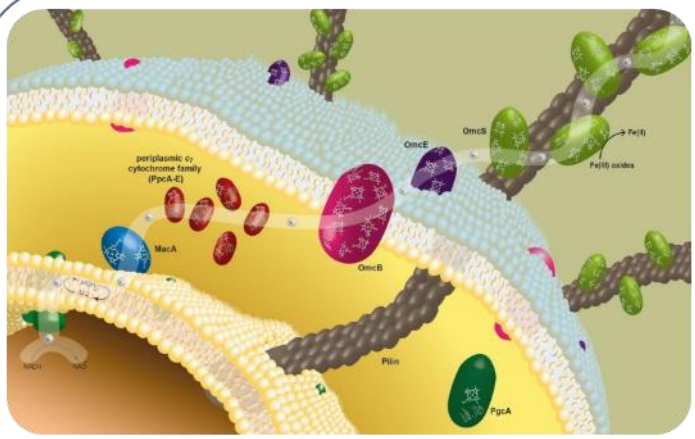

1. INTRODUCTION

1.1 Main features of the *Geobacter* bacteria

Geobacter species are Gram-negative bacteria that are capable to sustain their growth by using extracellular compounds as terminal electron acceptors, such as Fe(III), U(VI) or Mn(IV) oxides [1]. This contrasts with the more frequent bacterial respiratory processes that utilize both soluble electron donors (*e.g.* acetate) and acceptors (*e.g.* fumarate). Some of the referred extracellular compounds are toxic or radioactive, which makes *Geobacter* bacteria very appealing for biotechnological and bioremediation applications. The bioremediation strategies where these bacteria are involved include, for example (i) the stimulation of *Geobacter* growth by addition of an electron donor to the groundwater surfaces and encompasses, for example, the reduction of soluble U(VI) to insoluble U(IV) for the immobilization of uranium in contaminated ground waters [2, 3] or (ii) the anaerobic benzene degradation in petroleum-contaminated aquifers [4].

Furthermore, *Geobacter* species are highly effective in completely oxidizing organic compounds from aquatic sediments and waste organic matter to carbon dioxide under anaerobic conditions with the concomitant electron transfer to metals or to graphite electrodes in microbial fuel cells from which electricity can be harvested [2–4, 16]. *Geobacter* species produce higher current densities than any other known organism [1, 6]. However, at present, the power output of *Geobacter*-based microbial fuel cells is too low for most envisioned applications. Therefore, efforts toward the understanding of the *Geobacter* respiratory chain are expected to provide valuable information to improve the current-production by these bacteria [10].

1.2 *Geobacter sulfurreducens*

The genome of *Geobacter sulfurreducens* was fully sequenced and a genetic system developed [8, 9]. For these reasons *G. sulfurreducens* serves as a model to study the extracellular electron transfer mechanism in *Geobacter* spp [12, 13]. It was demonstrated by genetic studies that *G. sulfurreducens* synthesize a large number of *c*-type cytochromes, most of which are multiheme [6–8, 19]. These metalloproteins are involved in the control and coordination of important chemical events in cellular metabolism in bacteria and are particularly abundant in *Geobacter* species, suggesting that the electron transport pathways in these bacteria are extremely versatile, allowing

a precise and adequate physiological response to the diverse metal ions in the natural environments [17].

1.3 Extracellular electron transfer

Many of the terminal electron acceptors that can be used by *G. sulfurreducens* are insoluble and, thus, unable to diffuse inside the cells. Also, since these bacteria requires direct contact for reduction of the insoluble electron acceptors [18], it is not surprising that some of the most important proteins are located on the outer surface of the *G. sulfurreducens* cells and that electron transfer across the outer membrane is required once it cannot occur in the periplasm as in the case of soluble acceptors [13, 14]. In fact, besides the presence of multiheme cytochromes in the inner membrane and in the periplasm space, as in the majority of the microorganisms, multiheme cytochromes in *G. sulfurreducens* were also identified in the outer membrane [21]. Combining all this information, a model for the electron transfer to the extracellular acceptor Fe(III) in *G. sulfurreducens* was proposed (Figure 1).

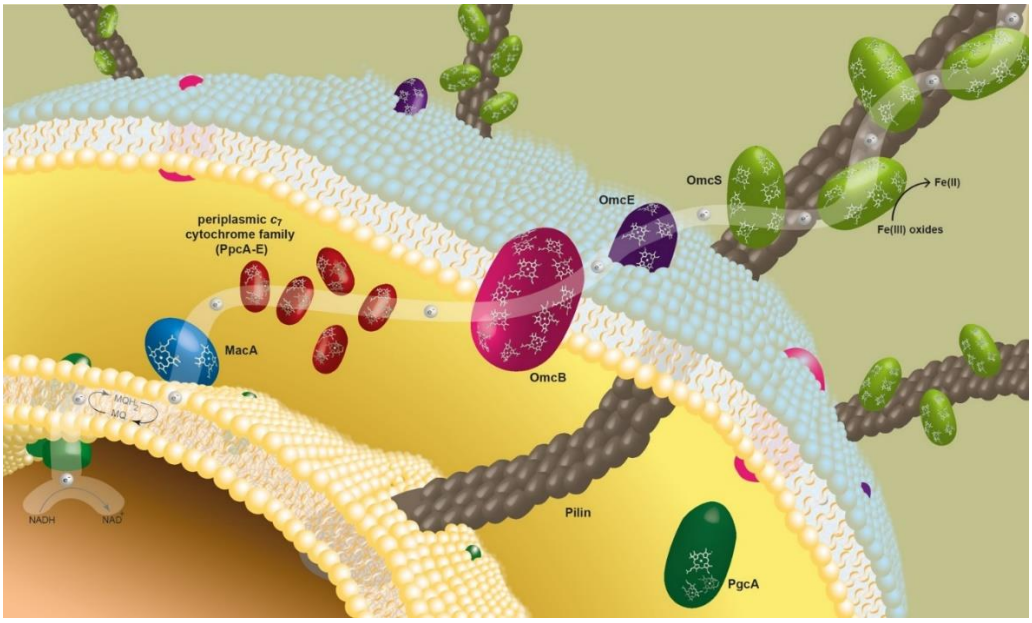

Figure 1. Proposed model for extracellular electron transfer pathway to Fe(III) oxides in *G. sulfurreducens*. The white path represents the proposed electron transfer pathway. The membrane associated cytochrome MacA receives electrons from the menaquinol (MQH_2)/menaquinone (MQ) pool at the inner membrane and reduces the periplasmic triheme cytochromes (PpcA-E). These cytochromes mediate the electron transfer from the periplasm to the outer membrane associated cytochromes (OmcB, OmcE and OmcS) that are likely to be directly involved in the reduction of insoluble Fe(III) oxides. OmcS was shown to be localized along the *pili* when *G. sulfurreducens*. Adapted from [22].

Although some of the cytochromes involved in the extracellular electron transfer in *G. sulfurreducens* were already identified, it is essential to obtain detailed characterization on such electron transfer components in order to not only elucidate these electron transfer mechanisms but also to promote new strategies to be explored in the improvement of the electricity production and in the design of optimal biotechnological applications [23].

1.4 *Geobacter metallireducens*

The bacterium *Geobacter metallireducens* was the first *Geobacter* species to be isolated and identified. This bacterium is capable of using different electron acceptors and donors, as described for *G. sulfurreducens*. It is an obligate anaerobic Fe(III)-respiring bacterium and was the first organism identified to be capable of: (i) conserve energy in order to support growth from the oxidation of organic compounds coupled with the reduction of Fe(III), Mn(IV) or U(VI); (ii) utilize humic substances as electron acceptors; (iii) remediate environments contaminated with aromatic compounds; (iv) more efficient Fe(III) reduction rates compared to *G. sulfurreducens* [24]. In contrast with *G. sulfurreducens*, *G. metallireducens* do not use fumarate as final electron acceptor. This latter is also able to convert nitrate to ammonia and to metabolize aromatic compounds [25]. Furthermore, the motility of *G. metallireducens* is one of the reasons that explain their high efficiency in the reduction of Fe (III) oxides compared to *G. sulfurreducens*. Nonetheless, as in *G. sulfurreducens*, the *c*-type cytochromes are important players in all these respiratory pathways [26].

1.5 Periplasmic triheme cytochromes from *G. sulfurreducens* and *G. metallireducens*

Despite the lack of information regarding the precise extracellular electron transfer mechanisms in both *G. sulfurreducens* and *G. metallireducens*, it is consensual that *c*-type cytochromes play a crucial role in those processes. These cytochromes contain at least one heme group, which is formed by a tetrapyrrole porphyrin ring coordinated to an iron atom. Cytochromes can be classified as type *a*, *b*, *c* or *d* according to the type of substituents at the periphery of the porphyrin ring [27]. In a *c*-type cytochrome the heme group, is covalently bound through thioether bonds to cysteine residues of the polypeptide chain arranged in a typical CXXCH motif (where X corresponds to any amino acid) and is composed by 20 proton-containing groups (four methyl groups, four meso proton, two thioether protons, two thioether methyl and two propionate groups – see Figure 2) [20, 21].

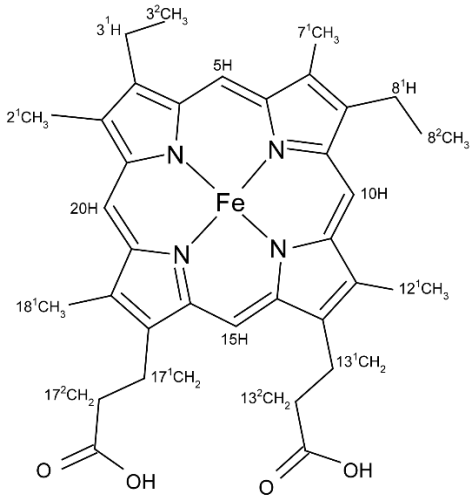

Figure 2. Representative structure of the *c*-type heme group accordingly to the IUPAC nomenclature [29]**.** The thioether bonds with the sulfur atom of cysteine residues in the heme binding motif are established with the carbons atoms harboring 3^1H and 8^1H groups. Adapted from [30].

A family composed by five triheme periplasmic *c*-type cytochromes with approximately 10 kDa each, designated by PpcA, PpcB, PpcC, PpcD, and PpcE was identified in *G. sulfurreducens*. It is believed that these five periplasmic proteins play an important role in the reduction of extracellular acceptors by bridging the electron transfer between the cytoplasm and cell exterior [23]. These periplasmic proteins, containing approximately 70 residues, show a high structural homology and share 77% (PpcB), 62% (PpcC), 57% (PpcD) and 65% (PpcE) amino acid sequence identity with PpcA [31]. A sequence alignment of these proteins is depicted in Figure 3A and shows that of the 21 highly conserved residues, only nine are not cysteine or histidine residues directly involved in heme binding. The five cytochromes have high isoelectric points (pI ≥ 9), due to the considerable content in lysine residues and all the heme groups are covalently linked to the polypeptide chain by two cysteine residues in a conserved CXXH binding motif.

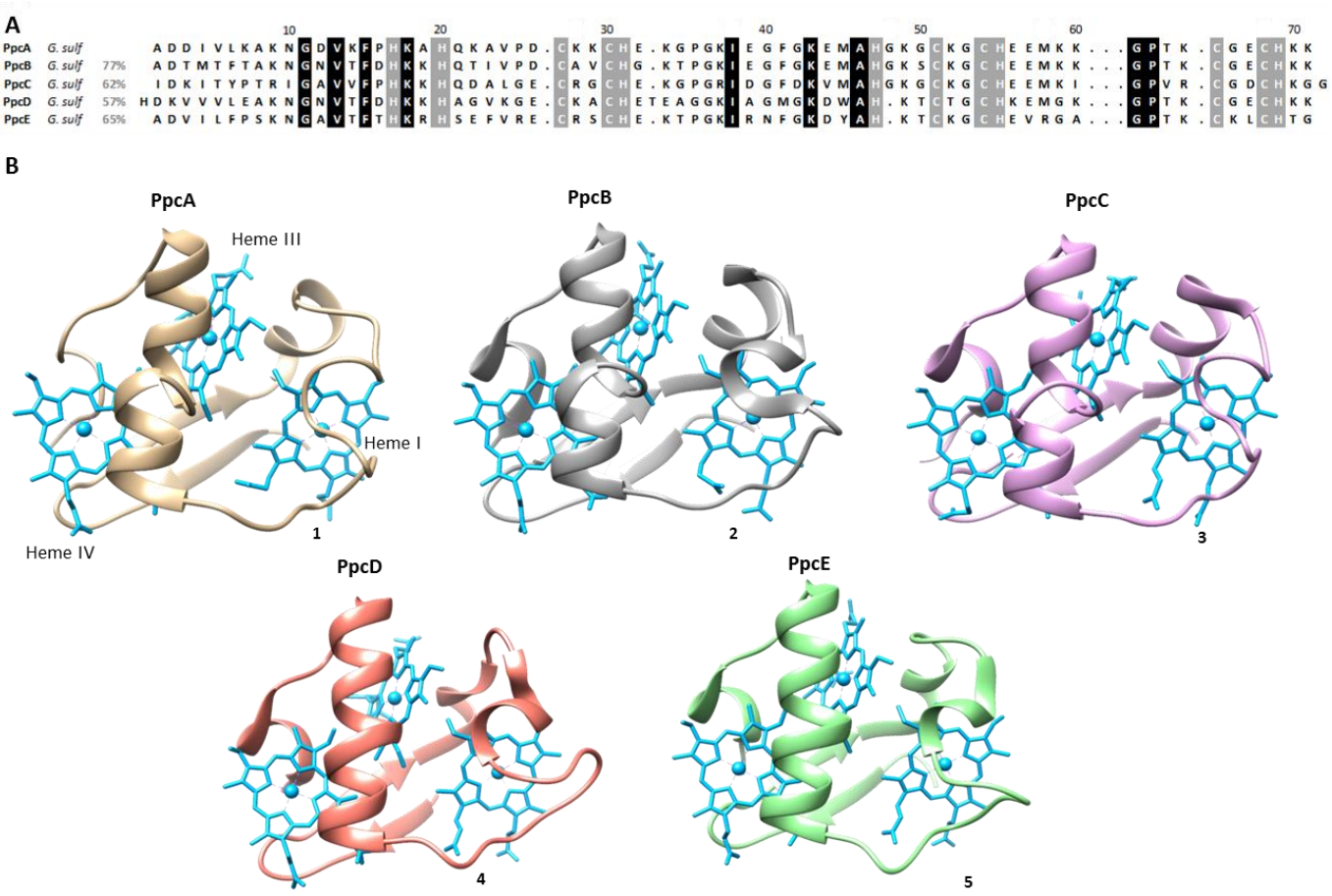

Figure 3. Alignment of the amino acid sequences and NMR (1) and crystal (2-5) structures of triheme cytochromes PpcA-E from *G. sulfurreducens*. (A) Sequence identity for each cytochrome of PpcA family from *G. sulfurreducens* in relation to PpcA. The conserved residues in the proteins are boxed: heme attached (gray) and non-heme attached residues (black). The specific heme and the respective attached residues are indicated on the bottom of the last cytochrome amino acid sequence. (B) 1) PpcA (PDB code 2LDO [32]); 2) PpcB (PDB 3BXU [33]); 3) PpcC (PDB 3H33 [34]); 4) PpcD (PDB 3H4N [34]); 5) PpcE (PDB 3H34 [34]). The molecules are all in the same orientation.

The crystal structures of these cytochromes have been determined and are indicated in Figure 3B. As depicted, the tertiary structure of all the proteins is similar, although local variations were observed. The spatial arrangement of the hemes in triheme cytochromes is superimposable with those of the structurally homologous tetraheme cytochromes c_3, with the sole difference being the absence of heme II and the corresponding polypeptide segment. For this reason, the heme groups have been numbered as I, III and IV. In these cytochromes all heme groups are axially coordinated by two histidine residues and are low-spin in both the reduced and oxidized forms. Therefore, they

are diamagnetic (Fe(II) and S = 0) and paramagnetic (Fe(III) and S = ½) in the reduced and oxidized states, respectively (Figure 4A). This feature is reflected in their UV-visible spectrum, here exemplified for PpcA in Figure 4B.

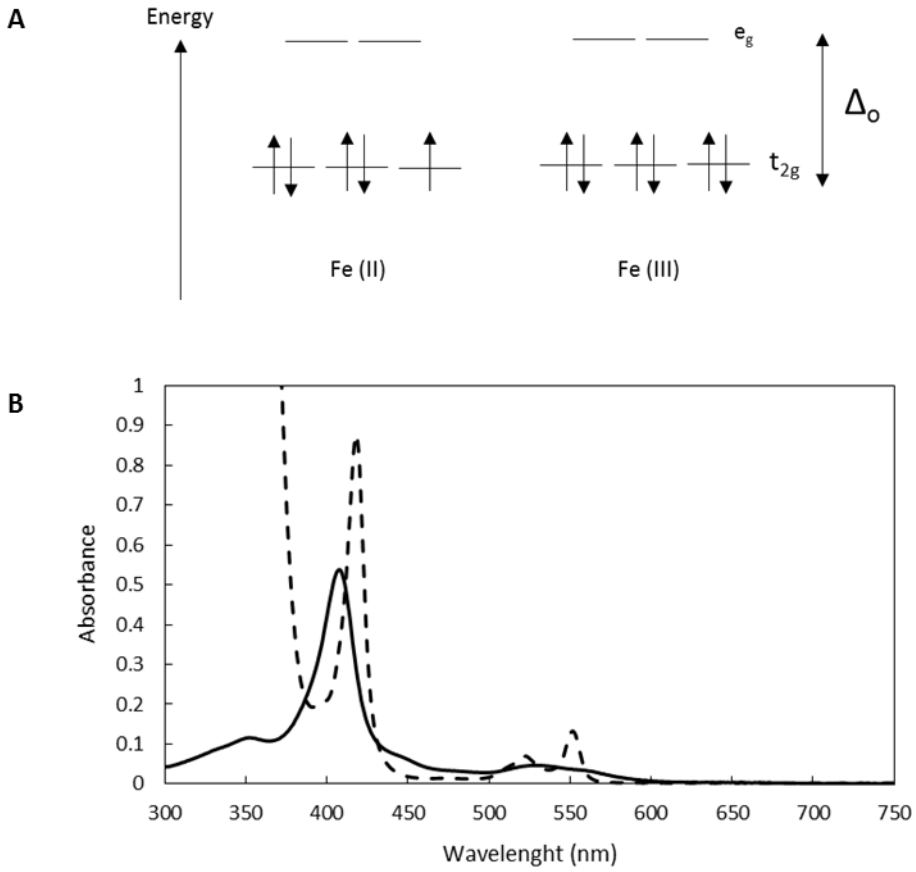

Figure 4. Electronic and spectroscopic properties of the heme iron in triheme cytochromes from *G. sulfurreducens*. (A) Spin-states of octahedral F(III) and Fe(II) at low spin state, where crystal field, Δ_o, is higher than the energy repaired to pair electrons in the same orbital, P (Δ_o>P). (B) Typical UV-visible absorption spectra. The oxidized form is represented by a solid line and is characterized by the Soret band with a maximum at 406 nm. In the reduced form (dashed line), three bands are observed: Soret band at 417 nm, β band at 522 nm and α band at 552 nm [35].

The thermodynamic properties of *G. sulfurreducens* PpcA family members, except for PpcC, have been determined showing that the redox potentials are negative and different for each cytochrome [26, 27]. A summary of these properties is indicated in Table 1.

Table 1. Midpoint heme reduction potentials (e_{app}) of PpcA, PpcB, PpcD and PpcE from *G. sulfurreducens* at pH 7.5 [26, 27]. Microscopic potentials are determined for each heme (I, III and IV). The redox potential values are relative to the standard hydrogen electrode (SHE).

Cytochrome	Reduction potentials (mV)		
	Heme I	Heme III	Heme IV
PpcA	-152	-108	-126
PpcB	-150	-155	-130
PpcD	-156	-102	-162
PpcE	-158	-158	-100

Similarly to the *G. sulfurreducens*, a family of five triheme periplasmic cytochromes, designated PpcA, PpB, PpcC, PpcE and PpcF was also found in *G. metallireducens* [24]. As depicted in Table 2, PpcF has relative little homology with PpcD, in fact it has the highest identity percentage with PpcA from *G. sulfurreducens*. For this reason, a new designation for this cytochrome was needed - PpcF. It was suggested that, as the PpcA family from *G. sulfurreducens*, the family of triheme cytochromes found in *G. metallireducens* is also involved in extracellular electron transfer [24]. However, none of these cytochromes were functional or structurally characterized to date.

Table 2. Sequence identity (%) between PpcA-family cytochromes from *G. sulfurreducens* and *G. metallireducens* [38].

		G. sulfurreducens				
G. metallireducens		**A**	**B**	**C**	**D**	**E**
	A	80	73	64	68	62
	B	68	72	57	68	63
	C	59	56	79	42	51
	E	54	61	52	55	69
	F	62	58	57	55	57

1.6 NMR basic principles

In general terms nuclear magnetic resonance spectroscopy (NMR) studies the absorption of electromagnetic radiation of a specific frequency by an atomic nucleus placed in a strong magnetic field. In fact, nuclei have positive charges and many behave as little spin bars. As known, anything that is charged and moves has a magnetic moment (μ) and produces a magnetic field (B). Therefore, a spinning nucleus acts as a magnet oriented along the spin rotation axis, called nuclear spin. In the presence of a much larger magnetic field the orientation of the spin will be no longer random, but the most favorable would be the low-energy state and the less favorable orientation the high-energy state.

Nuclei are characterized by a quantum spin number (I), which can be determined by its atomic mass. When I = 0, there is no nuclear spin and it is NMR silent. Most nuclei of biologic interest (e.g. ^{1}H, ^{13}C, ^{15}N, ^{19}F and ^{31}P) have nuclear spin quantum I = ½. The value of the quantum spin number determines the number of energy spin states that a nucleus may assume in presence of an external uniform magnetic field in accordance with the formula 2I+1. For a nuclei with I = ½, in the absence of an applied magnetic field (B_0) the two energy states are degenerated and the number of atoms in each state will be equal to the thermal equilibrium. On the other hand, in the presence of an external magnetic field the energy difference (ΔE) between the energy states α (m_I=+1/2, with the field) and β (m_I=-½, against the field) gives rise to the frequency of the spectra, whereas intensities of the signals are proportional to the population difference between α and β states. The ratio of the populations in the states is quantitatively described by the Boltzmann equation (Equation 1):

$$\frac{N_{\propto}}{N_{\beta}} = e^{\Delta E/k_B T} \qquad \textbf{(Equation 1)}$$

where N_{α} and N_{β} represents the number of nuclei in each possible spin orientation, k_B the Boltzmann constant and T the temperature.

The energy needed to induce the mentioned transitions between the states is the energy difference between the two states and depends of the magnetic field that is applied to the nuclei (Equation 2):

$$\Delta E = \frac{\gamma h B_0}{2\pi} \qquad \textbf{(Equation 2)}$$

where *γ* represents the gyromagnetic constant, which is constant to each nuclei and *h* represents the Planks constant.

Furthermore, in the presence of an external magnetic field, nuclei have an intrinsic frequency, which is known as the Larmor frequency (v_0), which is given by Equation 3. For instance, in a molecule, all protons have the same Larmor frequency. However, the signals of interest are those processing at frequencies slightly different from the Larmor frequency, an effect caused by the electron density surrounding each individual proton.

$$v_0 = \frac{\gamma B_0}{2\pi} \qquad \textbf{(Equation 3)}$$

In a sample, not all the nuclei are subject to the same chemical environment and that is reflected in a different chemical shift (δ), expressed in ppm (parts per million). The resonance frequencies are expressed in terms of an empirical quantity called chemical shift, which is related to the difference between the resonance frequency (v) of a nucleus in question and that of a reference standard (v_{ref}), Equation 4:

$$\delta = \frac{v - v_{ref}}{v_{ref}} 10^6 \qquad \textbf{(Equation 4)}$$

The approach to any structural or mechanistic problem will invariably start with the acquisition of one dimensional (1D) spectra, since these provide the foundations for further work. In a 1D experiment, the FID (free induction decay) is acquired after a radio frequency pulse or pulses, called the preparation period. A plot of the frequencies of the nuclei *versus* the signal intensities constitutes the 1D NMR spectrum. In the case of small molecules, the 1D spectrum can be sufficient to obtain the required information. Although, for a macromolecule this kind of spectra are too complex to be interpreted. In order to improve the spectral resolution for further studies, an additional dimension can be introduced to disperse the signals over two frequency dimensions, forming a multi-dimensional NMR spectrum. In the case of 2D NMR spectra, which were the most used in the current work, they include one additional period called the evolution time, which contains a variable time delay t_1, and is introduced between the preparation and acquisition periods. Moreover, the second dimension can be frequency for ^{1}H, which results in a square spectrum with diagonal peaks, or a heteronuclear acquisition, which gives asymmetric spectra. 2D experiments can also contain other periods in addition to the evolution time, such as a mixing time, t_m.

Finally, at the end of each experiment, all the FIDs are transformed with the same phase parameters followed by the calibration of the spectra. In the case of biological samples, it is common to calibrate the NMR spectra through the proton signal of the water (Equation 5):

$$\delta_{H_2O} = 5.11 - 0.012\,T \qquad \textbf{(Equation 5)}$$

where T represents the temperature of the experiment in degrees Celsius. The calibration of the other nuclei, such as ^{13}C and ^{15}N, is obtained by indirect referencing as described by Wishart and co-workers [39].

1.7 Functional and structural characterization of a triheme cytochrome: an overview

NMR is powerful technique in what concerns to the structural and functional characterization of a protein. However, in the particular case of multiheme cytochromes, the assignment of the protein signals is not a straightforward task, namely in the oxidized state. In fact, the paramagnetic effect of the unpaired electrons at the heme iron causes the spread and broadening of the signals of the heme groups, as well as those of the amino acid residues located in their neighborhoods, all over large spectral widths. In order to assist the solution structure determination and identification of molecular interactions the assignment of the protein signals, including those of the heme substituents is crucial.

The functional characterization of multiheme cytochromes typically encompasses the determination of their macro and microscopic redox properties, a task that benefits from the assignment of the heme methyl proton signals in the fully reduced and oxidized states. Therefore, the determination of the redox properties is also much more complex in multiheme cytochromes. In fact, in a monoheme cytochrome the variation of the protein reduced fraction with the solution potential can be calculated by the direct application of the Nernst equation (Equation 6)

$$E = E^0 + \frac{RT}{nF} ln \frac{[ox]}{[red]} \qquad \textbf{(Equation 6)}$$

This is possible because only two states co-exist in solution, the fully reduced and the fully oxidized (Figure 5). In this case, the solution redox potential for which the reduced and oxidized fractions of the protein are equal corresponds to the E_{app} value and therefore, to the reduction potential of the heme group.

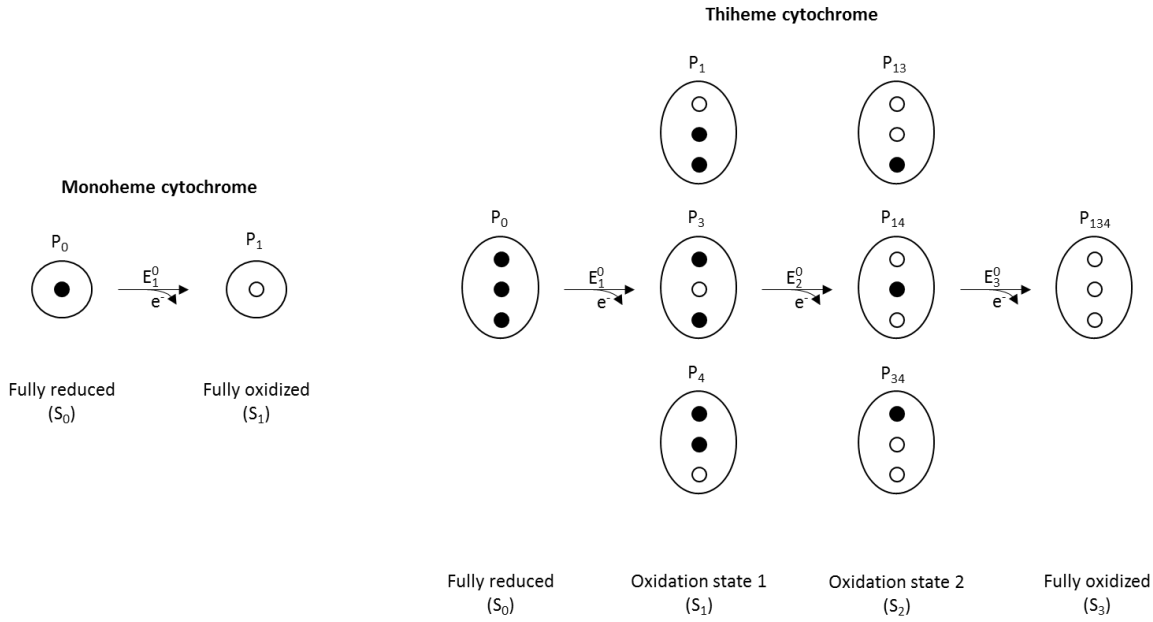

Figure 5. Electronic distribution scheme for monoheme and triheme cytochromes, showing the possible microstates in solution. The elliptic forms represent the cytochrome and the inner circles the heme groups, which can be either reduced (black circles) or oxidized (white circles). P represent the microstates and the followed number the hemes that are oxidized in that particular microstate.

In contrast, in the case of a triheme cytochrome, three consecutive reversible steps with the transfer of one electron convert the fully reduced state to the fully oxidized state (Figure 5). Therefore, four macroscopic redox stages are defined, and the relative populations of the four stages at equilibrium and three macroscopic reduction potentials (E_1^o, E_2^o and E_3^o) can be defined. These parameters can also be obtained by fitting the experimental variation of the total reduced fraction of the protein with the solution potential, as described below. It is worth noting that the macroscopic reduction potential values do not necessarily correspond to any of the heme groups.

Chapter 2: Characterization of triheme cytochrome PpcF from *G. metallireducens*

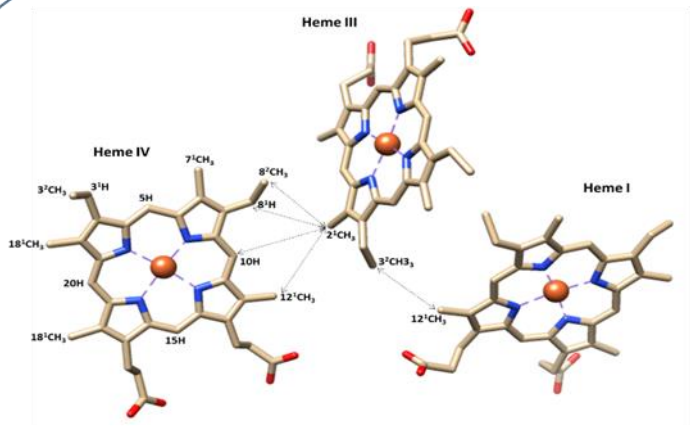

CONTEXTUALIZATION

G. metallireducens is a dissimilatory iron reducing bacterium that has the ability to utilize extracellular electron transfer acceptors, a feature that is shared by *G. sulfurreducens*. Tremblay and co-workers [26] identified a very important role for *pili* in the Fe(III) reduction and in the transfer of electrons to electrodes in *G. metallireducens*. The motility is one of the reasons why these bacteria are more efficient in the reduction of Fe (III) oxides compared to *G. sulfurreducens*. However the *c*-type cytochromes are important to this process as well [26]. To date, the components and mechanisms underlying the extracellular electron transfer in *G. metallireducens* are not yet fully elucidated [40]. This is a crucial step to contribute to the development of future applications in biofuel production and bioremediation.

Genetic and proteomic studies revealed that some *c*-type cytochromes appear to be overexpressed when the cells utilize nitrate as terminal electron acceptor. Such respiratory process was not observed for *G. sulfurreducens*. The nitrate reductase activity of *G. metallireducens* is attributed to the *narGYJI* genes. The gene *ppcF* (annotation number Gmet0335) of *nar* operon encodes a periplasmic triheme *c*-type cytochrome, designated PpcF, which is involved in this electron transfer pathway [24]. In fact, PpcF may permit the transfer of electrons to the nitrate reductase from extracellular electron donors such as humic substances or graphite electrodes [24].

As previously mentioned, PpcF is the one in the PpcA family from *G. metallireducens* that has little homology with the cytochrome PpcD from *G. sulfurreducens* the reason why it is not denominated PpcD. The lack of a homologous protein to PpcF in *G. sulfurreducens* makes PpcF more appealing to be studied. In order to contribute to the understanding of PpcF role we performed for the first time a biochemical characterization of this cytochrome.

2.1 MATERIALS AND METHODS

2.1.1 Protein expression

Escherichia coli BL21(DE3) cells were used to express the triheme cytochrome PpcF from *G. metallireducens*. *E. coli* cells, harboring the plasmid pEC86, which is a derivative from the pACYC184 containing the gene cluster needed to the cytochrome *c*, *ccmABCDEFGH*, [41] were transformed with the plasmid pCS0335, the expression vector containing the gene sequence encoding for PpcF. Transformed *E. coli* cells were grown aerobically in 2xYT rich media supplemented with 34 µg/mL chloramphenicol (CLO) and 100 µg/mL ampicillin (AMP), both from NZYTech. Colonies were selected and grown in 50mL 2xYT medium (also supplemented with 34 µg/mL CLO and 100 µg/mL AMP) to a $1.8<OD_{600nm}<2$, at 30 °C, 200 rmp, overnight. 20% of this culture was transferred to 1L of 2xYT media (34 µg/mL CLO and 100 µg/mL AMP) and grown till they reach an $OD_{600nm}>1.5$, at 30 °C and 200 rpm. At this stage, protein expression was induced with 10 µM isopropyl β-D-1-thiogalactopyranoside (IPTG) from NZYTech and incubated overnight at 30 °C and 160 rpm. Then, cells were harvested and centrifuged at 6400 *g* for 20 min at 4 °C, to isolate the periplasmic fraction. The cell pellet was gently resuspended in 30 mL of lysis buffer, per liter of initial cell culture, constituted by: 20 % sucrose (VWR), 100 mM Tris-HCl (NZYTech) pH 8, 0.5 mM EDTA (Amresco) and 0.5 mg/mL lysozyme (Fluka). The suspension was incubated at room temperature during 15 min, then 15 min on ice with gently shaking and finally centrifuged at 14700 *g*, 20 min, at 4 °C. The resulting supernatant was ultracentrifuged at 44000 *g*, 1 h, at 30 °C. The resulting supernatant was dialyzed (MWCO 3500) against 10 mM Tris-HCl pH 8.

2.1.2 Protein purification

PpcF was purified using first a cation exchange chromatography and then a molecular exclusion chromatography. Dialyzed protein was injected in a cation exchange 2x5 mL GE Healthcare HiTrap SP HP column equilibrated with 10 mM Tris-HCl pH 8 and the cytochrome was eluted with a 0-300 mM NaCl, 150 mL length, gradient in 10 mM Tris-HCl, at a flow rate of 1 mL/min. The collected red fractions were concentrated to 1 mL and injected in a Superdex 75 molecular exclusion column (GE Healthcare) of 120 cm, equilibrated with 100 mM sodium phosphate buffer, pH 8, and eluted at a flow rate of 0.5 mL/min. Both chromatography steps were performed on an ÄKTA Prime Plus FPLC

System (GE, Amersham). Protein purity was evaluated by sodium dodecyl sulfate polyacrylamide gel electrophoresis (15%), stained with Coomassie brilliant blue (Sigma).

2.1.3 UV-visible analysis, quantification and molar extinction coefficient determination

UV-visible absorption spectra were acquired for the obtained purified cytochrome on a UV-visible scanning spectrometer Thermo scientific Evolution 201 with quartz cuvettes with 1 cm path length (Helma), at room temperature. Fully sample reduction was achieved by adding sodium dithionite (Sigma) in small increments. Protein concentration was determined by measuring the absorbance of the reduced PpcF α-band at 552 nm, using the extinction coefficient of 87.4 $mM^{-1}cm^{-1}$ determined in this work by the Pierce BCA Protein Assay Kit (Thermo Scientific). This method consists in a detergent-compatible formulation based on bicinchoninic acid (BCA) for the colorimetric detection and quantification of total protein. It combines the well-known reduction of Cu^{+2} to Cu^{+} by protein in an alkaline medium, known as the biuret reaction, with the highly sensitive and selective colorimetric detection of the cuprous cation (Cu^{+}). Then the chelation of two molecules of BCA with one cuprous ion results in purple-colored reaction product. This water-soluble complex exhibits a strong absorbance at 562nm that is nearly linear with increasing protein concentrations over a broad working range (20-2000µg/mL). As standard it was used PpcA from *G. sulfurreducens*. Afterwards UV-visible spectra of PpcF was recorded in the range 350-700 nm, at room temperature for both oxidized and reduced samples and used to determine the molar extinction coefficient of the cytochrome.

2.1.4 Molecular mass determination

The theoretical molecular mass of cytochrome PpcF was calculated taking into account the amino acid composition of the mature protein and the molecular mass of three heme *c* groups. The experimental mass of cytochrome PpcF was determined by matrix-assisted laser desorption-ionization time-of-flight mass spectrometry (MALDI-TOF-MS) using a Voyager-DE™ PRO Biospectrometry Workstation equipped with a nitrogen laser radiating at 337 nm from Applied Biosystems (Analysis laboratory Requimte – LAQV/UCIBIO). A matrix solution of sinapinic acid in 70:30 water/acetonitrile with 0.1% TFA (final concentration) was used. The measurements were

performed in triplicated in positive ion mode using ProteoMass™ cytochrome *c* MALDI-MS from Sigma-Aldrich (MW 12361.96 Da) as internal calibration.

2.1.5 Heme quantification

Heme quantification of cytochrome PpcF was performed using the pyridine hemochrome method described by Berry and Trumpower [42]. 5 µM of purified PpcF in aqueous solution was incubated with 50mM NaOH and 20% v/v pyridine at room temperature for 15 minutes. The solution was separated in two fractions. One fraction was reduced with sodium dithionite (pyridine ferrohemochrome form) whereas the other was oxidized with potassium ferricyanide (pyridine ferrihemochrome form). UV-visible spectra were acquired between 350-700 nm for both fractions. The number of hemes was calculated using the absorption coefficient of 21.84 $mM^{-1}cm^{-1}$ for the α-band in the pyridine ferrohemochrome sample, using Equation 7 [42],

$$A = [Heme] \times l \times \varepsilon_{550nm}$$

$$Number\ of\ heme = \frac{[Heme]}{[PpcF]} \qquad \textbf{(Equation 7)}$$

where A represents the visible absorption, l the length of the light path in cm and ε the absorption coefficient.

2.1.6 Redox titrations followed by visible spectroscopy and determination of reduction potentials

Redox titrations of PpcF were followed by visible spectroscopy at 15 ºC inside an anaerobic glove box (MBraun) with oxygen conditions <1 ppm. 30 µM samples of the protein in 20 mM NaCl were prepared in 80 mM sodium phosphate with NaCl (250 mM final ionic strength). Each redox titration was performed in the reductive and in the oxidative direction, allowing inferring about the occurrence of hysteresis. Sodium dithionite and potassium ferricyanide solutions were used to reduce and oxidize the samples, respectively. The following mixture of redox mediators was added to the solution with a final concentration of approximately 1.5 µM, as described in the literature [43], to ensure the equilibrium between the redox center of the protein and the working electrode: methylene blue, gallocyanine, indigo trisulfonate, indigo tetrasulfonate, indigo disulfonate, anthraquinone-2,6-disulfonate, 2-hydroxy-1,4-naphthoquinone, safranine O, diquat, benzyl viologen, neutral red and methyl viologen. These mediators cover the potential range of 280 to -120

mV (relative to standard hydrogen electrode, SHE). A combined Pt/Ag/AgCl electrode was used for measuring the solution potential. The redox potential of the solution was measured after each addition of reductant or oxidant agent, and once stable, a visible spectrum was recorded.

The experiments were performed at least twice at each pH value, and the reduction potentials were found to be reproducible within +/- 5 mV. The reduced fraction of the protein was determined by integrating the area of the α-peak (552 nm) above the line connecting the flanking isosbestic points (545 and 559 nm) to subtract the optical contribution of the redox mediators, as described previously [33]. Each measured solution redox potential value were corrected to the standard hydrogen electrode reference by the addition of 207 mV. The macroscopic reduction potential values for cytochrome PpcF were determined by fitting the observed reduced fraction to the Equation 8 (section 2.2.5).

2.1.7 NMR studies

NMR spectra were acquired in a Bruker Avance III 600 spectrometer equipped with a triple-ressonance cryoprobe (TCI). All NMR spectra were processed using TOPSPIN (BrukerBiospin, Karlsruhe, Germany) and analyzed with Sparky (TD Goddard and DG Kneller, Sparky 3, University of California, San Francisco, USA). ^{1}H chemical shifts were calibrated using the water signal as internal reference and the ^{15}N and ^{13}C chemical sifts were calibrated through indirect referencing [39].

2.1.7.1 Determination of the heme core architecture

Cytochrome PpcF samples with approximately 0.5 mM for 2D NMR studies were prepared in 80 mM sodium phosphate pH 8 and pH 7 buffer with NaCl (250 mM final ionic strength) in $^{2}H_2O$. To assist the heme signal resonance assignments 2D-^{1}H NOESY (nuclear overhauser effect spectroscopy) with 80 ms mixing time and spectral width of 14 kHz and 2D-^{1}H TOCSY NMR spectra with 60 ms mixing time and spectral width of 14 kHz, were acquired for the fully reduced cytochrome (pH 7 and 8, 15 ºC). The fully reduction of cytochrome PpcF was achieved by first flushing out the air from the oxidized sample with argon. NMR sample was reduced directly in the NMR tube with gaseous hydrogen in the presence of catalytic amounts of hydrogenase from *Desulfovibrio vulgaris*, as previously described [33]. For the fully oxidized cytochrome 2D-^{1}H NOESY

with 80 ms mixing time and spectral width of 41 kHz, 2D-^{1}H TOCSY (total correlation spectroscopy) with 45 ms mixing time and spectral width of 41 kHz and 2D-^{1}H,^{13}C HMQC (heteronuclear multiple quantum coherence) with spectral width of 41 kHz in F_2 and 250 in F_1 NMR spectra were acquired (pH7, 15 and 25 °C). The spectra were acquired by collecting at 4k and at least 256 scans per increment.

2.1.7.2 Assignment of the heme substituents in the reduced and oxidized states

In the reduced state, the first step to assign the heme substituents signals is the analysis of the connectivities between a thioether methine (3^{1}H or 8^{1}H) and a thioether methyl group ($3^{2}CH_3$ or $8^{2}CH_3$) in the 2D-^{1}H TOCSY NMR spectrum, as depicted in Figure 6. Indeed, these are the only protons that are part of the same spin system and, therefore can be easily detected in such NMR experiments.

On the other hand, 2D-^{1}H NOESY experiments allow detecting spatial correlation between nuclei that are typically closer than 5 Å. Thus, as also depicted in Figure 6, meso protons present a characteristic pattern of short-range intraheme connectivities: protons H15 are not connected to either methyl groups or thioether substituents; protons H20 are connected to two heme methyls ($2^{1}CH_3$ and $18^{1}CH_3$); and the only ambiguity arises from H5 and H10 protons, which both present connectivities with a thioether methine, a thioether methyl and one heme methyl group. This ambiguity was solved by observing the connectivities between one of the heme methyls near the H20 protons ($2^{1}CH_3$ and $18^{1}CH_3$) with the closest tioether methyl ($3^{2}CH_3$), which were unequivocally assign in the 2D-^{1}H TOCSY. This allowed connecting H20 and H5 faces of each heme. The heme methyls $7^{1}CH_3$ are part of H5 faces and also show connectivities with thioether groups (8^{1}H and $8^{2}CH_3$), which are in H10 faces. After the identification of these three heme faces, H15 protons were identified by observing the connectivities between cross-peaks that connect H15 and $12^{1}CH_3$ or $18^{1}CH_3$ protons (Figure 6).

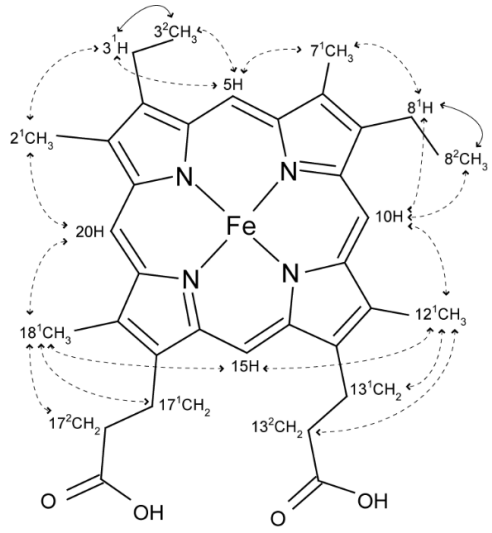

Figure 6. Diagram of heme *c* numbered according to the IUPAC-IUB nomenclature [29]**.** The typical through bond connectivities are indicated by solid arrows, whereas the dashed ones indicate the typical NOE connectivities used to assign the heme substituents. Adapted from [30].

In the paramagnetic oxidized state, in addition to the ring-current effects, the intrinsic (from own heme) and the extrinsic (from neighboring hemes) paramagnetic contribution due to the presence of unpaired electrons strongly contributes to the final observed chemical shift of the heme substituents, making their assignment more complex. In fact, in the oxidized form the same type of signals are differently affected by the paramagnetic centers, show different levels of broadness and are spread all over the entire NMR spectral width. Therefore, the chemical shifts of the heme substituents in the oxidized form are completely different in comparison with those observed in the fully reduced proteins. Consequently, a different NMR assignment strategy was used to assign the heme signals in the oxidized form. In this case, 2D-^{1}H,^{13}C HMQC NMR experiment is very useful to map some of the heme substituent signals because typical ^{1}H,^{13}C regions can be identified. The propionates αCH_2 protons ($17^{1}CH_2$ and $13^{1}CH_2$) are identified in ^{1}H,^{13}C HMQC NMR spectrum, whereas the intraheme connectivities with the propionates βCH_2 ($17^{2}CH_2$ and $13^{2}CH_2$) are obtained from the analysis of 2D-^{1}H TOCSY spectrum and then confirmed in 2D-^{1}H,^{13}C HMQC NMR spectra at the typical region of propionates βCH_2. Afterwards, in 2D-^{1}H NOESY spectra we identified the cross peaks of each propionate proton with those of the closest heme methyl ($18^{1}CH_3$ and $12^{1}CH_3$).

2.1.7.3 Identification of the order of oxidation of the heme groups

The oxidation patterns of the heme groups of PpcF in 80 mM sodium phosphate with NaCl (250 mM final ionic strength) in $^{2}H_2O$ were monitored by acquiring a series of 2D-^{1}H EXSY (exchange spectroscopy) NMR experiment at pH 7 and 16 ºC, with the sample poised at several degrees of oxidation. All spectra were acquired with a mixing time of 25 ms and 256 scans per increment.

In a triheme cytochrome, three consecutive reversible steps of one-electron transfer convert the fully reduced state (stage S_0) in the fully oxidized state (stage S_3), as described in Figure 5. Therefore, four different redox stages can be defined that comprise 8 microstates. When the intramolecular electron transfer exchange (between microstates within the same oxidation stage) is fast on the NMR time scale and the intermolecular exchange (between microstates belonging to different oxidation stages) is slow, on the NMR time scale, the individual heme NMR signals can be discriminated [33, 34]. In this case, the heme oxidation fractions can be determined from the chemical shifts of their heme substituents in the different oxidation stages. In fact, the distribution of paramagnetic shifts observed for each oxidation stage is governed by the relative microscopic reduction potentials of the heme groups, and thus provides information on the relative order of oxidation of the hemes.

The heme methyl resonances are the easiest identifiable NMR signals amongst the heme substituents, making them ideal candidates to monitor the stepwise oxidation of the hemes. Indeed, as show below in sections 2.2.7 and 2.2.8, the chemical shift of the heme signals are considerably different in the reduced and oxidized states, shifting from crowded regions in the fully reduced to relatively empty regions in the fully oxidized spectra. Therefore, as the oxidation of the multiheme cytochrome proceeds, the heme methyl signals become much shifted from the diamagnetic region of the spectra and the signals can be followed during a redox titration monitored by 2D-^{1}H EXSY NMR spectra.

2.2.1 Purification of PpcF from *G. metallireducens*

After the expression of PpcF, the protein was sequentially purified by cation exchange chromatography and molecular exclusion chromatography. The elution profiles obtained for both chromatographic steps are represented in Figures 7 and 8, respectively.

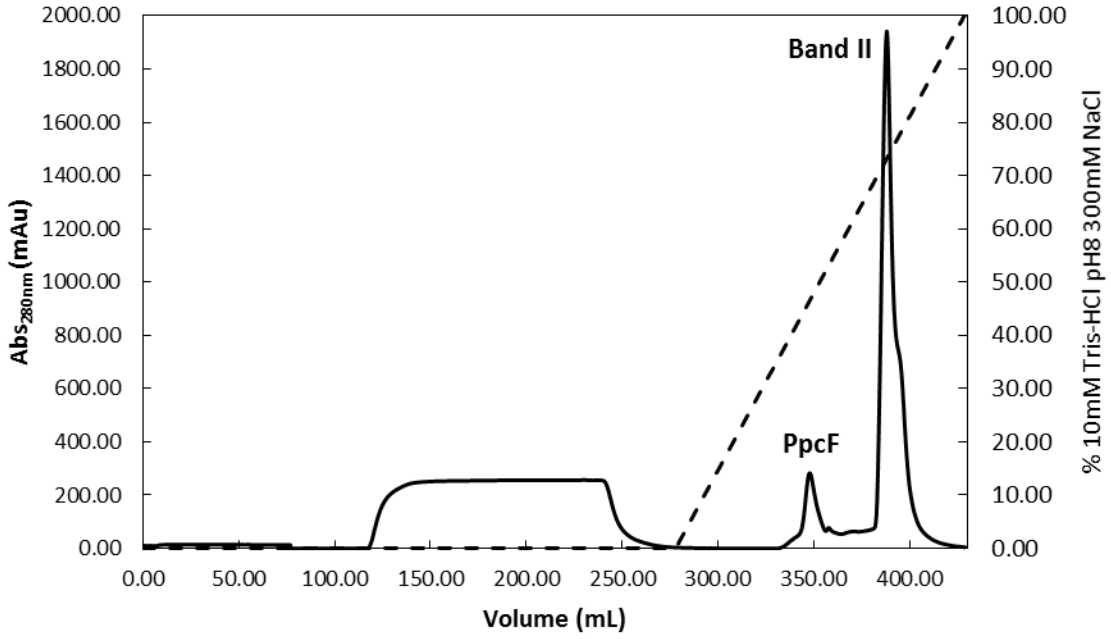

Figure 7. Elution profile for the cation exchange chromatography of PpcF from *G. metallireducens*. Cation exchange chromatography column equilibrated with 10 mM Tris-HCl pH 8. Elution at 1 mL/min flow rate. Solid line corresponds to the variation of absorbance at 280 nm. Dashed line reports the NaCl gradient profile.

Based on the amino acid sequence of PpcF an isoelectric point of 8.96 was determined using the pI/Mw tool program on the ExPASy Server. Taking into consideration this value, the cytochrome was purified using a cation exchange chromatography column previously equilibrated with 10 mM Tris-HCl pH 8. In these conditions the cytochrome binds to the column and was eluted by the linear increase of the buffer ionic strength. As indicated in the Figure 7, the protein of interest, which presents a red characteristic color typical for proteins containing heme groups, was eluted at approximately 46% (138.9 mM) of the ionic strength gradient.

With this first purification step the majority of the contaminants were removed. However it was necessary to complement it with a molecular exclusion chromatographic step. The elution profile obtained in the molecular exclusion chromatography is represented in Figure 8. PpcF was eluted at approximately 88 mL.

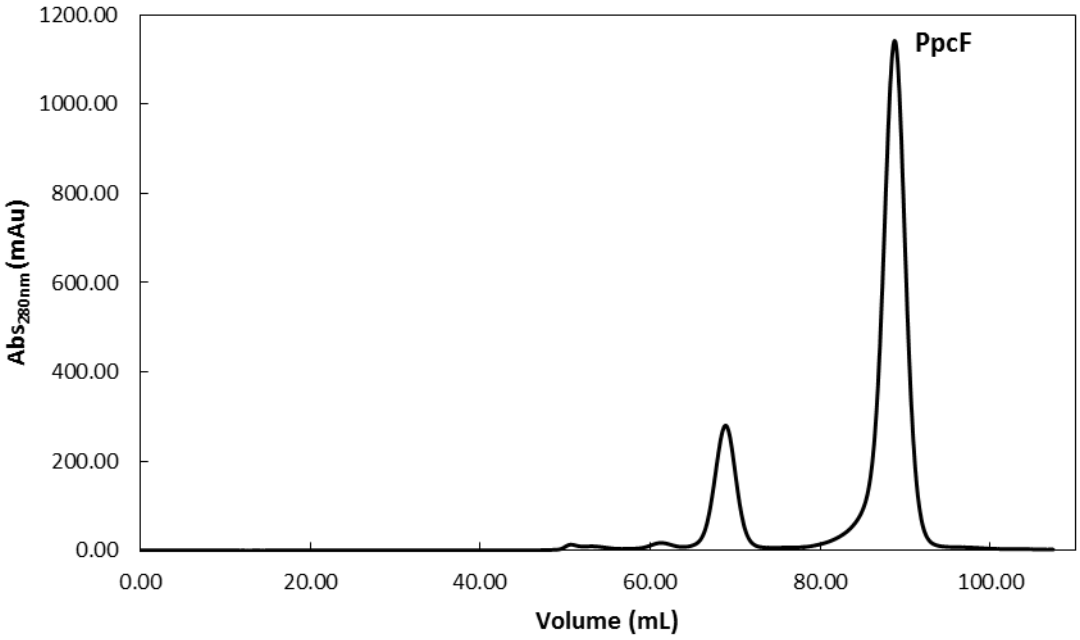

Figure 8. Elution profile for the molecular exclusion chromatography of PpcF from *G. metallireducens*. Molecular exclusion chromatography column equilibrated with 100 mM sodium phosphate buffer, pH 8, with a flow rate of 0.5 mL/min.

The fraction corresponding to the PpcF band were analyzed by SDS-PAGE electrophoresis (Figure 9) and MALDI-TOF-MS (Figure 10) to infer about its purity. The SDS-PAGE electrophoresis gel (Figure 9) shows one intense band in the expected MW region (≈10 kDa), after the final purification step. Also, the second and highest band observed in the cation exchange chromatography (Band II, see Figure 7) which presents a brownish color was analyzed by SDS-PAGE electrophoresis and corresponds to proteins with lower molecular weight compared to PpcF.

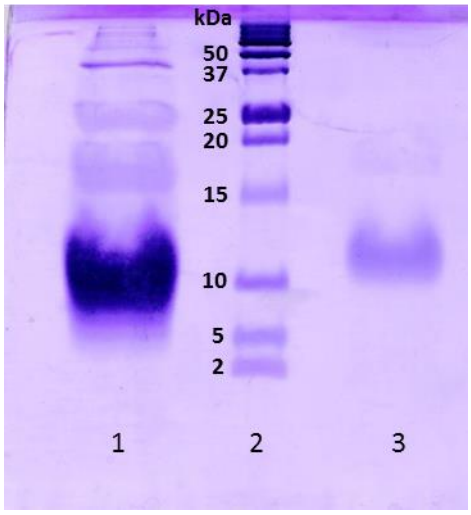

Figure 9. Purity analysis by SDS-PAG electrophoresis of PpcF from *G. metallireducens*. Obtained results of SDS-PAGE gel, 15% acrylamide, stained with Coomassie brilliant blue. Lane 1) Band II obtained in the cation exchange chromatography; Lane 2) Protein marker (Protein Plus Protein Dual Xtra Standards, Bio-Rad, appendix A1; Lane 3) Purified fraction after molecular exclusion chromatography. The molecular weights of the protein markers are in indicated on the left of lane 2.

2.2.2 Molecular weight determination

The mass spectrum obtained for the purified fraction of PpcF (Figure 10) indicates a molecular mass of 9737.13 ± 0.002 Da, which is in excellent agreement with the calculated one using the *Compute pI/Mw tool* [46] (7886.21 Da from the mature protein plus three times 616.5 Da from the three heme groups, yielding a total molecular mass of 9735.71 Da). This result also confirms that PpcF has three heme groups.

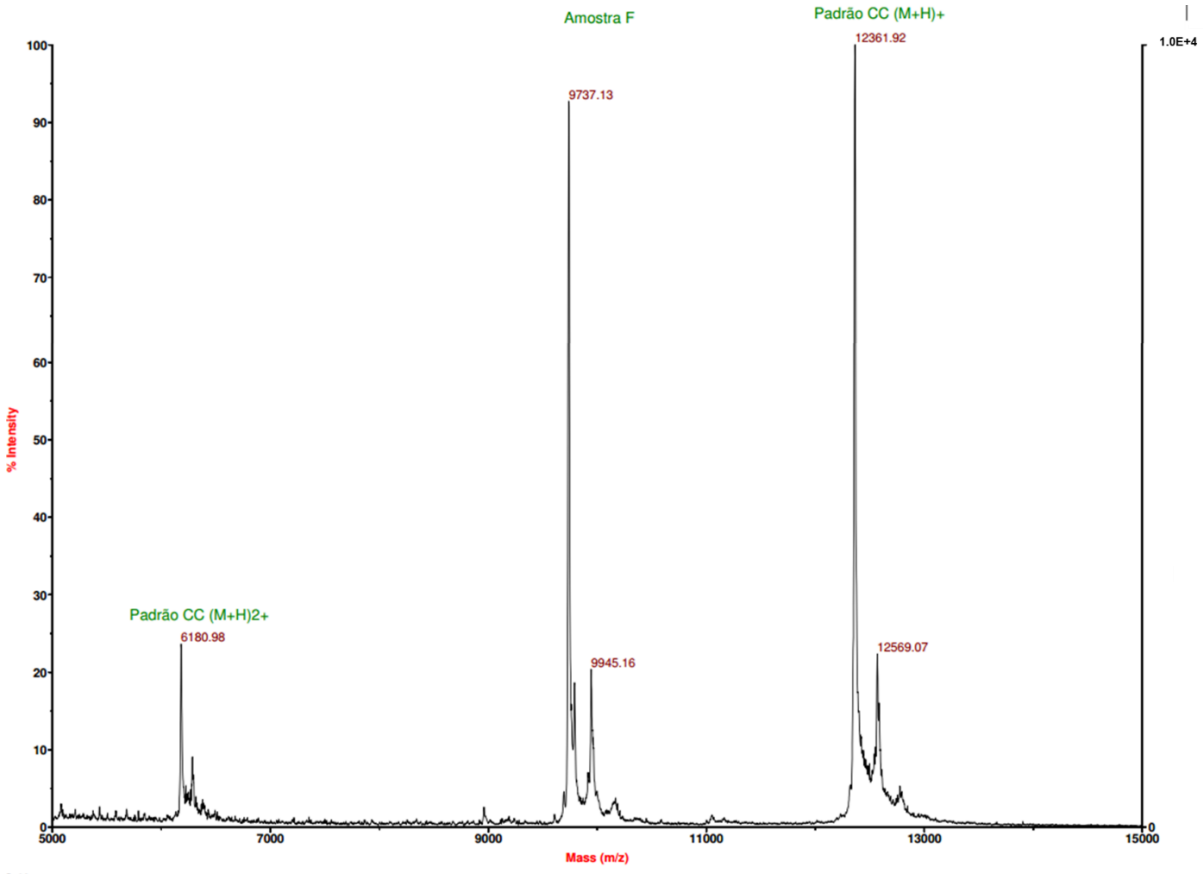

Figure 10. Mass spectrum obtained by MALDI-TOF method of PpcF from *G. metallireducens*. Analysis of the sample was performed in a Voyager-DE^{TM} Pro Workstation, with positive ionization mode, using sinapinic acid as matrix. Pattern CC $(M+H)^+$ represents a sample of horse cytochrome *c* that was used as internal calibration.

2.2.3 Molar extinction coefficient determination

The molar extinction coefficient of cytochrome PpcF was determined with the BCA Protein Assay (Thermo Scientific Piece). The calibration curve obtained is indicated in Figure 11, using cytochrome PpcA from *G. sulfurreducens* as standard. The value of ε_{552nm} = 97.5 $mM^{-1}cm^{-1}$ [36] was used to calculate the concentration of PpcF samples in the reduced form. From this study it was possible to determine a value of ε_{552nm} = 87.4 $mM^{-1}cm^{-1}$ for the PpcF molar extinction coefficient.

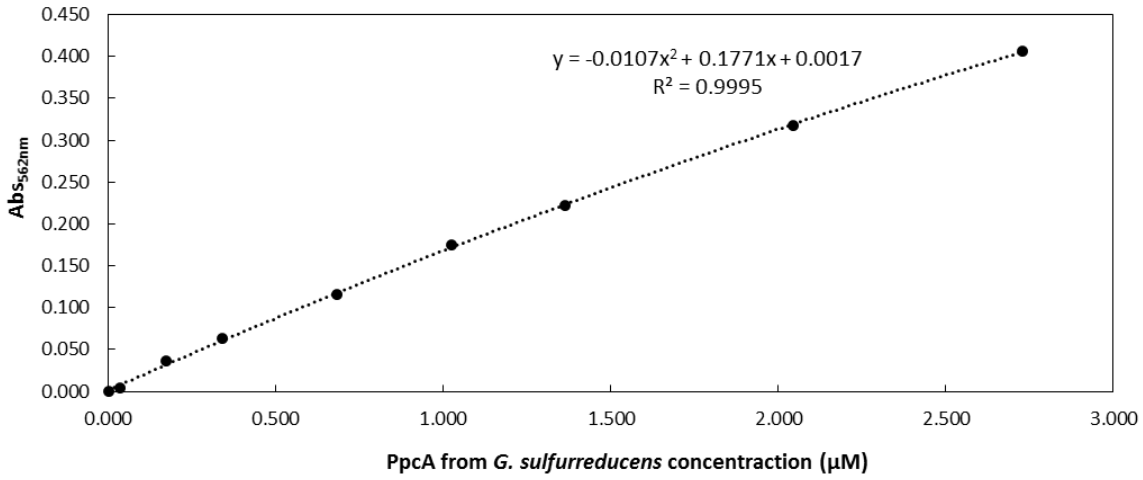

Figure 11. Calibration curve obtained for cytochrome PpcA from *G. sulfurreducens* using the BCA method. The parameters correspondent to the calibration line are indicated as an inset together with its accuracy (R^2).

2.2.4 Heme quantification

Pyridine hemochrome method was used to further confirm the number of hemes present in PpcF cytochrome. An absorbance of 0.330 at 550 nm was obtained in presence of sodium dithionite. Based on the molar extinction coefficient correspondent to this wavelength (30.27 $mM^{-1}cm^{-1}$ [42]) it was possible to determine a heme content of 3.1 per cytochrome and confirm that PpcF has three heme groups.

2.2.5 Redox titrations of cytochrome PpcF followed by UV-visible spectroscopy

The redox titrations followed by UV-visible take advantage of the spectroscopic properties of heme proteins. In Figure 12, the UV-visible spectra of PpcF in both oxidized and reduced states are shown. In the oxidized state only a prominent band is observed at 410 nm, whereas in the reduced state three bands 419 nm (Soret), 523 nm (β) and 553 nm (α) are observed. For this reason the α-band was selected to monitor the reduction fraction of the protein in the redox titrations.

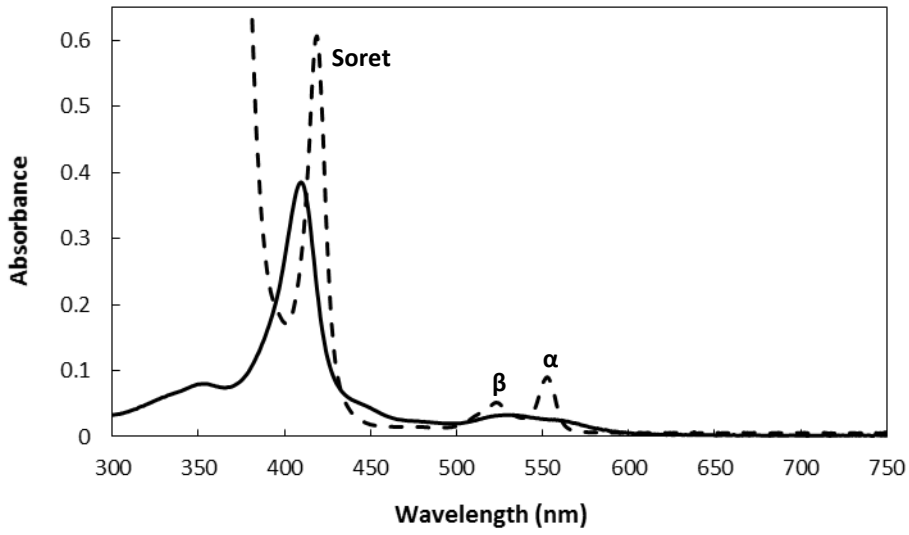

Figure 12. UV-visible absorption spectra of triheme cytochrome PpcF. The oxidized spectrum is represented by a solid line and the Soret band appears at 410nm. In the reduced spectrum (dashed line), three bands are observed: Soret at 419nm, β at 523nm and α at 553nm.

The redox titrations of PpcF from *G. metallireducens* were performed at two different pH values (pH 7 and 8) and are indicated in Figure 13.

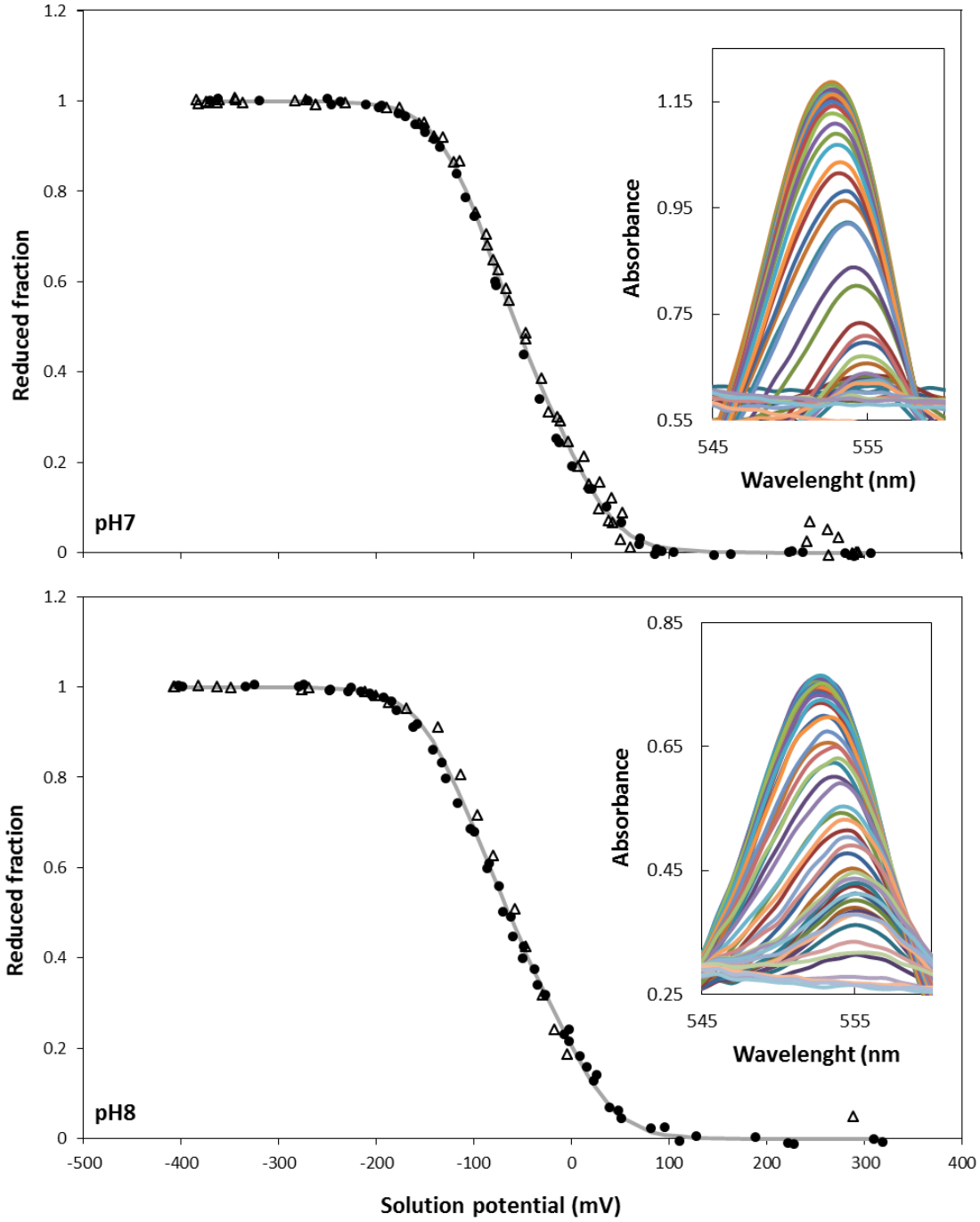

Figure 13. Redox titration curves for PpcF from *G. metallireducens* (15 °C and pH 7 and 8). The circles and triangles represent the oxidation and reduction directions, respectively. The grey line represents the fitting curve resulting from Equation 8. The insets represent an expansion of the α-band region. In these insets each line represents a different experimental measurement. The isosbestic points were 559 and 544 nm for pH 7 and 560 and 545 nm for pH 8.

The values of the macroscopic reduction potentials (E_1^o, E_3^o and E_4^o) were determined by fitting the Equation 8 (see appendix 2) to each experimental data set. In this equation it was considered one electron exchange between the different redox states (n = 1) and the following values: F = 96500 $Cmol^{-1}$, R = 8.314 $JK^{-1}mol^{-1}$ and T = 288.15 K.

$$Reduced\ Fraction = \frac{3 + 2e^{\left[(E-E_1^o)\times\frac{F}{RT}\right]} + e^{\left[(2E-E_1^o-E_3^o)\times\frac{F}{RT}\right]}}{3\times\left(1 + e^{\left[(E-E_1^o)\times\frac{F}{RT}\right]} + e^{\left[(2E-E_1^o-E_3^o)\times\frac{F}{RT}\right]} + e^{\left[(2E-E_1^o-E_3^o-E_4^o)\times\frac{F}{RT}\right]}\right)}$$

(Equation 8)

The adjustment of the experimental reduced fraction values were obtained using the Solver tool from Microsoft Excel software and the three macroscopic reduction potentials, as well as the apparent midpoint potential value (E_{app}), for both pH values are indicated in Table 3. The values obtained for the PpcA family members from *G. sulfurreducens* are also included in Table 3 for comparison.

Table 3. Macroscopic reduction potentials (*versus* SHE) and apparent midpoint potentials for PpcF from *G. metallireducens* (this work) and for PpcA family cytochromes from G. sulfurreducens (PpcA, PpcB, PpcD and PpcE).

Cytochrome	pH 7				pH 8			
	E_{app} (mV)	E_1^0 (mV)	E_2^0 (mV)	E_3^0 (mV)	E_{app} (mV)	E_1^0 (mV)	E_2^0 (mV)	E_3^0 (mV)
PpcF	-56	-108	-59	10	-64	-125	-66	6
PpcA [27, 32]	-117	-171	-119	-60	-138	-182	-139	-93
PpcB [27, 32]	-137	-185	-140	-84	-143	-192	-145	-103
PpcD[37]	-132	-181	-133	-78	-148	-191	-152	-94
PpcE [37]	-134	-191	-133	-82	-139	-194	-138	-85

Overall, the reduction potential values obtained for PpcF are clearly more positive than the ones observed in the PpcA family from *G. sulfurreducens*. There are several factors that control the reduction potentials in multiheme cytochromes [47]. From these factors, heme solvent accessibility, charge distribution and redox-interactions between the heme groups are the most important ones [48]. Unfortunately, the solution structure of PpcF is not available and therefore the structural features that explain the observed differences could not yet be identified. Once available, the

structure of PpcF will allow us to determine the heme solvent accessibilities, map the spatial distribution of the charged residues that can possibly influence the reduction potential of the protein and measure the distances between the heme irons.

The difference in the apparent midpoint reduction potential (E_{app}), obtained from the visible redox titrations carried out at pH 7 and 8 for PpcF (Table 3) also indicates that the properties of the individual redox centers are affected by the pH of the solution (redox-Bohr effect). This might be important and provide a role for PpcF in the energy transduction processes in *G. metallireducens*.

2.2.6 1D-^{1}H NMR spectral features of PpcF

As mentioned above, the 1D-^{1}H NMR spectra of PpcF show important differences in the reduced and in the oxidized states (Figure 14). Both spectra present well dispersed and narrow signals which indicate the correct fold of the protein. NMR is a very powerful technique to identify the spin state of the heme groups, since the signals appear in quite distinct spectral regions for cytochromes with hemes in the high- or low-spin state. High-spin cytochromes in the oxidized state show 1D-^{1}H NMR spectra with extremely broad signals above 40 ppm, which typically correspond to the heme methyls substituents. On the other hand, in low-spin cytochromes, the methyl signals are mostly found in the 8-35 ppm region. In the reduced form, 1D-^{1}H NMR spectra are also distinct in both spin states, since cytochromes in high-spin show wider spectral regions (commonly from -15 up to 30 ppm) in comparison with the low-spin ones (frequently from -5 to 10 ppm). Therefore, 1D-^{1}H NMR spectra of PpcF in both oxidation states shows typically patterns of low-spin hemes. In fact, in the oxidized state, the spectrum covers the region between -5 e 25 ppm, while in the reduced state, the spectrum only covers the region between -2 and 11 ppm. Therefore, the protein is diamagnetic when reduced (Fe(II), S = 0) and paramagnetic when oxidized (Fe(III), S = ½).

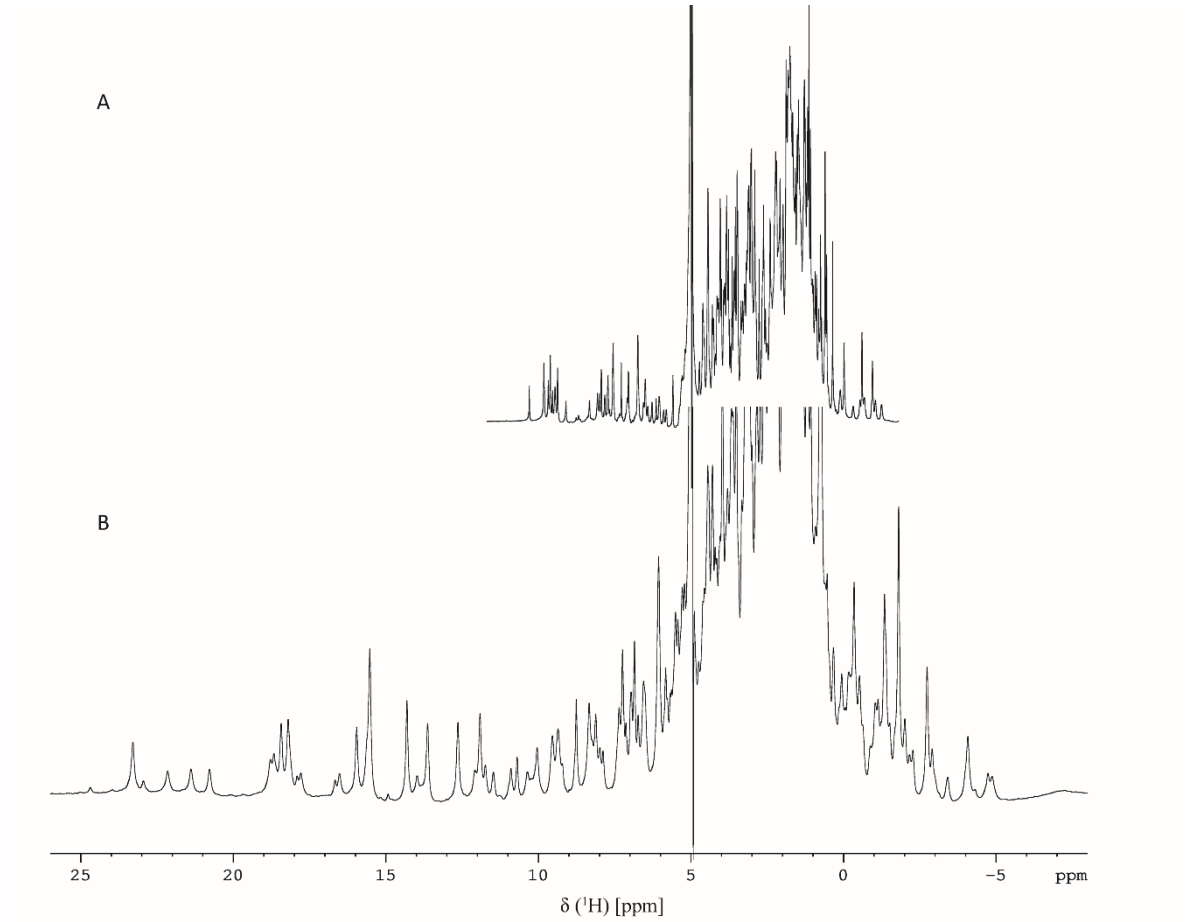

Figure 14. 1D-^{1}H NMR spectra of cytochrome PpcF from *G. metallireducens* (15 °C and pH 7) in the reduced (A) and oxidized (B) states.

2.2.7 Assignment of the heme substituents of cytochrome PpcF in the reduced state

The heme substituent proton signals of PpcF from *G. metallireducens* in the reduced state were assigned through the strategy previously described (see section 2.1.7.2) and their chemical shifts are listed in Table 4.

Table 4. Chemical shifts (ppm) of PpcF heme protons in the reduced state (15 °C and pH 7). The values obtained at pH 8 and 15 °C are indicated in parenthesis.

Heme substituent	Chemical shifts (ppm)		
	Heme I	Heme III	Heme IV
5H	9.42 (9.41)	9.77 (9.73)	9.06 (9.01)
10H	9.41 (9.39)	9.78 (9.75)	9.33 (9.29)
15H	9.42 (9.30)	9.51 (9.54)	9.58 (9.53)
20H	9.64 (9.60)	10.26 (10.23)	9.57 (9.53)
2^1CH_3	3.42 (3.39)	4.42 (4.39)	3.73 (3.70)
7^1CH_3	3.56 (3.55)	3.46 (3.92)	3.06 (3.02)
12^1CH_3	3.07 (3.09)	3.51 (3.48)	3.80 (3.75)
18^1CH_3	3.61 (3.58)	4.00 (3.98)	3.45 (3.42)
3^1H	5.85 (5.81)	6.68 (6.63)	6.01 (5.96)
8^1H	6.52 (6.48)	6.47 (6.43)	6.24 (6.21)
3^2CH_3	2.18 (2.16)	2.52 (2.48)	2.04 (2.01)
8^2CH_3	1.94 (1.92)	3.00 (2.97)	1.49 (1.46)

The observed cross peaks between the heme signals in the 2D-^{1}H NOESY spectra allowed to infer about the heme core architecture of PpcF. As mentioned above, PpcF shows the highest degree of sequence homology with PpcA from *G. sulfurreducens* (Table 2). Therefore, taking as reference the heme core of PpcA (Figure 15), the NOE connectivities observed between the PpcF heme signals indicates that the heme core architectures of both proteins are similar.

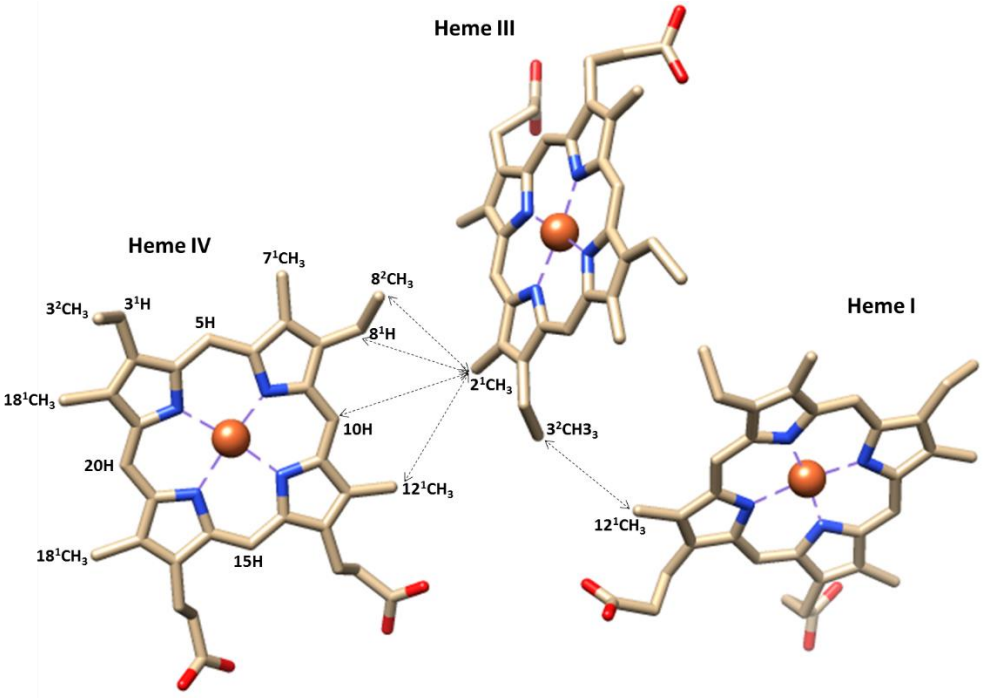

Figure 15. NOE connectivities observed between the heme proton signals of PpcF from *G. metallireducens*. The NOE connectivies are indicated by the dashed lines. The heme core represented corresponds to that of PpcA from *G. sulfurreducens* (PDB code: 2LDO).

2.2.8 Assignment of the heme substituents of cytochrome PpcF in the oxidized state

The heme propionate and methyl signals of PpcF from *G. metallireducens* in the oxidized state were assigned through the strategy previously described (section 2.1.7.2). The chemical shifts of the assigned signals are listed in Table 5.

Table 5. ^{1}H and ^{13}C chemical shifts (ppm) of the heme propionate and methyl groups of PpcF in the oxidized state (pH 7 at 25 °C and 15 °C). The resonances not detected are indicated by "n.d." The blue numbers indicates the lowest and the highest ^{13}C shift for the heme propionate groups.

T (°C)	Group	Heme I		Heme III		Heme IV	
		^{13}C	^{1}H	^{13}C	^{1}H	^{13}C	^{1}H
25	2^{1}	-36.26	17.97	-25.13	12.40	-22.88	11.85
	7^{1}	-18.08	6.86	-36.36	15.37	-29.50	13.56
	12^{1}	-52.41	22.70	-30.04	17.93	-32.96	14.22
	13^{1}	-15.07	8.08	-60.53	21.21	-17.90	7.44
			0.70		20.10		2.72
	13^{2}	88.09	-0.93	166.50	-1.88	95.10	-0.34
			-1.79		-2.51		-0.88
	17^{1}	-7.17	2.48	-13.68	4.98	-19.92	4.86
			0.94		3.09		4.50
	17^{2}	73.90	-0.92	84.59	-2.08	95.81	-0.52
			-1.29		-2.67		-1.47
	18^{1}	-38.30	16.08	-2.84	1.71	-35.57	15.50
15	2^{1}	-38.43	18.42	-26.71	12.63	-24.21	11.91
	7^{1}	-18.93	6.49	-36.50	15.51	-30.89	13.62
	12^{1}	-54.98	23.28	-31.42	18.19	-34.38	14.30
	13^{1}	-16.91	8.22	-63.83	21.39	-19.66	7.23
			0.34		20.76		2.49
	13^{2}	89.47	-1.08	171.4	-2.05	97.34	-0.58
			-2.03		-2.79		-1.05
	17^{1}	-8.15	2.03	-15.23	2.711	-21.30	4.38
			0.33		n.d.		n.d.
	17^{2}	73.65	-1.16	85.79	-2.30	97.35	-0.64
			-1.54		-2.93		-1.71
	18^{1}	-39.64	15.96	-2.91	1.12	-37.74	15.53

As in the reduced state, the analysis of the NOE connectivities between the heme substituents signals corroborates the conserved heme core architecture in PpcF and PpcA from *G. sulfurreducens*. This was further confirmed by the unusual high and low value of the ^{13}C chemical shift observed for the C_{α} and C_{β} from $13^{1}CH_{2}^{III}$ propionate group, respectively (see blue numbers in Table 5). In fact, for all members of PpcA family triheme cytochromes in *G. sulfurreducens*, only the $13^{1}CH_{2}^{III}$

propionate groups show these quite distinct chemical shifts for C_α and C_β [38, 39], a feature that arises from the particular heme core architecture that is conserved in this family of cytochromes (see Figure 3).

2.2.9 Order of oxidation of the heme groups

The chemical shift of the heme proton methyl groups obtained for PpcF in the oxidized and reduced state are possible starting points to monitor the oxidation profiles of the individual hemes as the protein oxidation progresses. This is possible when the intra- and inter-molecular electron transfer exchange rates are fast and slow, on the NMR scale, respectively (see section 2.1.7.3). This was the case of PpcF and, therefore several 2D-^{1}H EXSY NMR spectra were acquired with samples in intermediate levels of oxidation (examples of these spectra are indicated in Figure 16). The heme oxidation order can be obtained by the oxidation profile of one methyl per heme [44]. However, the selected methyls should point to the surface of the protein in order to minimize the extrinsic contribution due to the oxidation of neighboring hemes to the observed paramagnetic shift [44]. Therefore, the oxidation of the hemes in PpcF is monitored by the oxidation profiles displayed by methyls $2^1CH_3^{I}$, $12^1CH_3^{III}$ and $18^1CH_3^{IV}$.

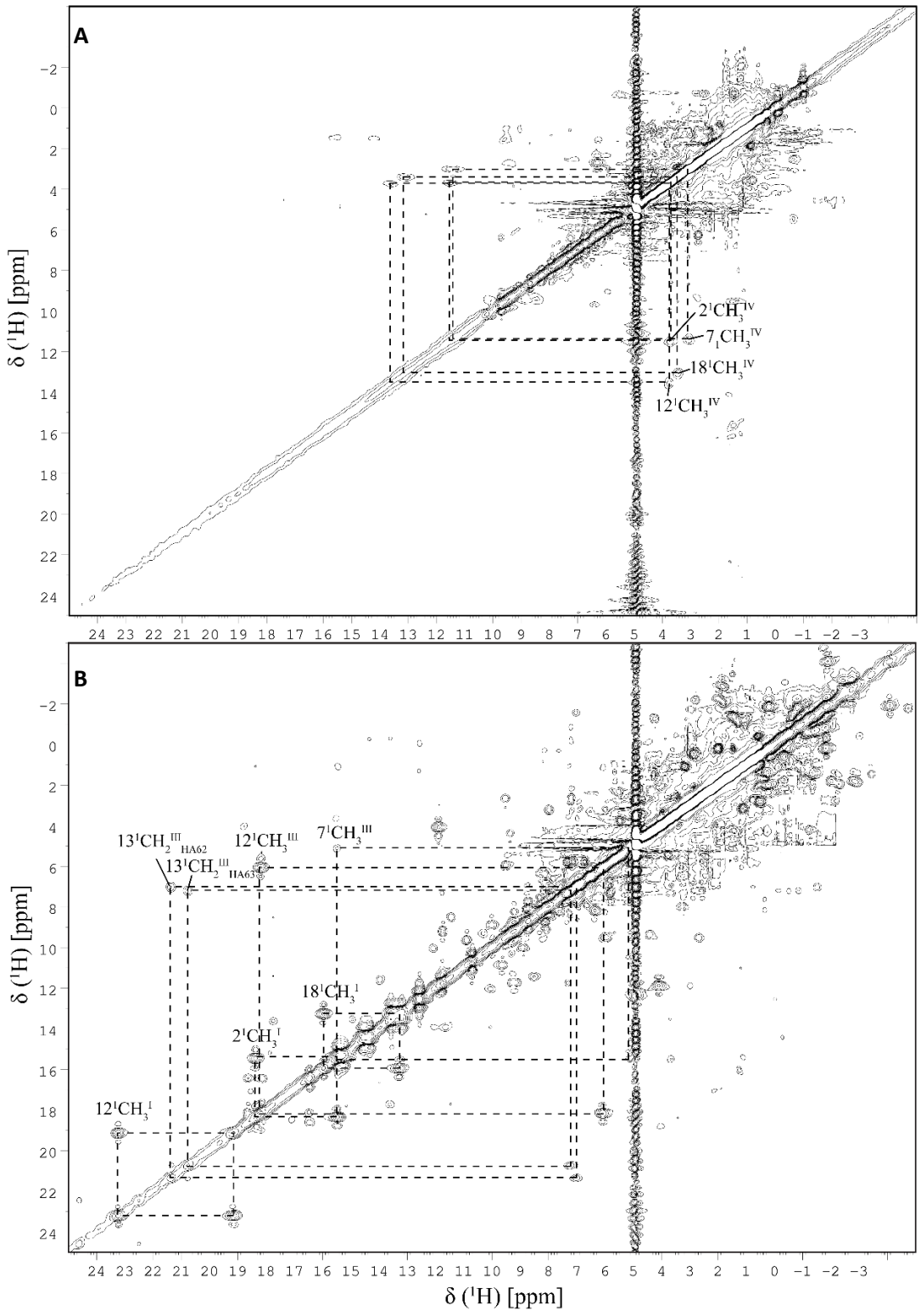

Figure 16. 2D-^{1}H EXSY NMR spectrum of PpcF obtained at intermediated oxidation levels (15 °C and pH 7). (A) Early stages of oxidation. (B) Later stages of oxidation. Cross peaks connecting the chemical shifts of heme methyls in different oxidation stages are indicated by dotted lines. The Roman numbers indicate the heme group.

For the spectra acquired in early stages of oxidation only the connectivities connecting the chemical shifts of the heme IV methyls in oxidation stages 0 and 1 could be observed (Figure 16A). This is illustrated by the chemical shift of the heme methyl $12^1CH_3^{IV}$ in Table 6 and the correspondent oxidation fractions in Table 7. In this case, heme IV oxidizes by approximately 80% in the first oxidation step, which indicates that this step is dominated by the oxidation of heme IV. Such significant amount of oxidation also explains why exchange connectivities for the other hemes could not be observed. The exchange connectivities for the signals of heme I and III are only observable at higher stages of oxidation, as illustrated in Figure 16B. Since the level of oxidation is too high to permit the observation of the connectivities with the stage 0 signals, the assignment of exchange connectivities for hemes I and III was carried out using the assignment of the heme methyls in the fully oxidized state (Table 5). The chemical shifts connecting the heme methyl signals $2^1CH_3^{I}$ and $12^1CH_3^{III}$ of PpcF in different oxidation stages are listed in Table 6 and the corresponding oxidation fractions in Table 7.

Table 6. Chemical shifts of the heme methyl $2^1CH_3^{I}$, $12^1CH_3^{III}$ and $12^1CH_3^{IV}$ of PpcF in the four oxidation stages (15 °C and pH 7). The resonances not detected are indicated by "n.d.".

Oxidation stage	Heme I	Heme III	Heme IV
	2^1CH_3	12^1CH_3	12^1CH_3
0	3.42	3.51	3.80
1	n.d.	n.d.	13.68
2	15.48	6.11	15.20
3	18.42	18.19	14.30

Table 7. Oxidation fractions, x_i, of the PpcF heme groups (16 °C and pH 7). The oxidation fraction resonances not determined are indicated by "n.d.".

Oxidation stage	x_i			Σx_i
	$2^1CH_3^{I}$	$12^1CH_3^{III}$	$12^1CH_3^{IV}$	
0	0.0	0.0	0.0	0
1	n.d.	n.d.	0.804	n.d.
2	0.804	0.177	0.920	1.901
3	1.0	1.0	1.0	3

As indicated in Table 7, the first stage of oxidation is dominated by heme IV (approximately 80%). On the other hand, the last step of oxidation is dominated by the oxidation of heme III (approximately 80%). Since both hemes I and III can oxidized at maximum 20% in the second oxidation step, this is dominated by the oxidation of heme I. Therefore, the order of oxidation of the heme groups in PpcF is IV-I-III.

2.3 CONCLUSIONS

In order to characterize the triheme cytochrome PpcF from *Geobacter metallireducens* the protein was firstly successfully heterologously expressed and purified with a protein yield of 0.94 mg per liter of culture.

The molecular weight of PpcF was determined by MALDI-TOF spectrometry and the results were in agreement with the expected theoretical mass of 9737 Da. The number of hemes present in the cytochrome was also quantified and the expected number of heme groups per protein (3) was confirmed.

The UV-visible spectra of PpcF displayed the typical features of *c*-type cytochromes containing low-spin heme groups. In the oxidized state the spectra showed one intense band at 410 nm, whereas for the reduced form, three bands are observed: Soret (419nm), β (523nm) and α (553nm). Furthermore, the molar extinction coefficient of PpcF was determined (87.4 $mM^{-1}cm^{-1}$).

The apparent midpoint macroscopic potential (E_{app}) of PpcF was determined at pH 7 (-56 mV) and pH 8 (-64 mV). The values obtained are considerably higher compared to the ones observed for the PpcA family from *G. sulfurreducens*. These differences can be probably attributed to structural and residue content differences, resulting in different heme solvent accessibility and nearby charge distribution. Also, the differences observed in the values obtained at pH 7 and 8 indicates that the protein displays a redox-Bohr effect at physiological pH.

The 1D-^{1}H NMR spectra of PpcF further confirmed the spin state of the cytochrome. In both states, the dispersion of the signals covered regions that are typical for low-spin cytochromes. Hence, the cytochrome is diamagnetic when reduced (Fe(II), S = 0), and paramagnetic when oxidized (Fe(III), S = ½).

The assignment of PpcF heme substituent signals was carried out in both reduced and oxidized states. The analysis of the NOE connectivities between the assigned signals indicated that the architecture of the heme core is conserved in PpcF and PpcA family in *G. sulfurreducens*.

The individual heme oxidation profiles were studied via 2D-^{1}H EXSY NMR experiments and the obtained data allowed us to establish the order of oxidation of the heme groups: IV – I – III.

Chapter 3: Molecular interactions between *G. sulfurreducens* triheme cytochromes and the electron acceptor Fe(III) citrate studied by NMR

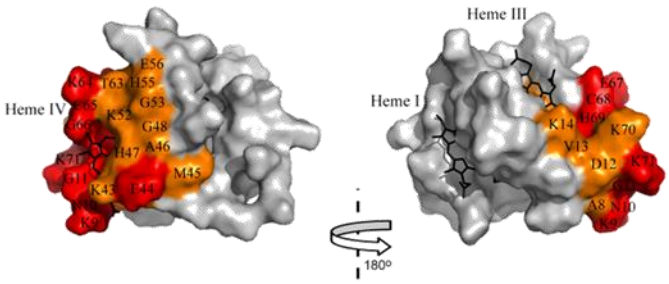

CONTEXTUALIZATION

As previously mentioned, the *Geobacteracea* family display a considerable respiratory versatility. Beyond, the most common soluble electron acceptors such as fumarate, these bacteria have the ability to reduce soluble toxic metal oxides of Cr(VI) and radioactive contaminants like U(VI) to the corresponding insoluble forms, which has an important impact in the bioremediation field.

Geobacter multiheme cytochromes have been implicated in the extracellular electron transfer pathway used by the microorganism to reduce soluble or insoluble iron complexes. Previous studies demonstrated that PpcA, PpcB and PpcD were found in both Fe(III) citrate and Fe(III) oxide cultures, but PpcA abundance was statistically similar under both culturing conditions, while PpcB was more abundant during growth on Fe(III) citrate [51]. In contrast, PpcD was the only showing higher abundance in the Fe(III) oxide supplanted cultures. PpcE was only detected in cultures with Fe(III) citrate. Also, genetic studies have suggested that PpcA is an important component in Fe(III) citrate reduction [52].

The fact that three triheme cytochromes (PpcA, PpcB and PpcE) are involved in the *G. sulfurreducens* Fe(III) citrate respiratory pathways, constitute a good model to understand how multiheme cytochromes can possible interact with this electron acceptor [9–11]. In the present work we used NMR measurements to investigate whether Fe(III) citrate interacts with each cytochrome and to fingerprint the regions involved in the interaction between the two molecules. The results of these experiments allow us to present for the first time structural evidence for molecular interaction between Fe(III) citrate and PpcA, PpcB and PpcE, which constitutes an important step to understand this respiratory pathway in *G. sulfurreducens*.

3.1 MATERIALS AND METHODS

3.1.1 Protein expression

The triheme cytochromes PpcA and PpcB from *G. sulfurreducens*, both unlabeled and isotopic labeled, and PpcE unlabeled, were already available expressed and purified in the laboratory prior to the start of this thesis. As previously described in the section 2.1.1 for the expression of PpcF, PpcE from *G. sulfurreducens* was heterologously expressed in *Escherichia coli* BL21(DE3) cells.

To ^{15}N isotopic labelling PpcE the followed protocol has some differences from the one used to produce unlabeled PpcF (section 2.1.1). After the cells reach the mid-exponential phase (OD_{600nm}>1.5), cultures were harvested by centrifugation at 6400 *g*, 30 min. The resultant cell pellet was washed twice with 250 mL of a salt solution containing 43 mM NaCl (Panreac), 240 mM Na_2HPO_4 (VWR Chemicals) and 110 mM KH_2PO_4 (Riedel-de-Haën). Afterwards, cells were resuspended in 250 mL minimal media composed by 34 µg/mL CLO, 100 µg/mL AMP, 8.6 mM NaCl, 48 mM Na_2HPO_4, 22 mM KH_2PO_4, 20 mg/L biotin (Fagron), 20 mg/L vitamin B1 (Fluka), 2 mM $MgSO_4{\cdot}7H_2O$ (Panreac), 0.1 mM $CaCl_2$ (Sigma-Aldrich), 5 µM $MnCl_2{\cdot}4H_2O$ (VWR), 10 µM $FeSO_4{\cdot}7H_2O$ (Merck), 1 mM of the heme precursor δ-aminolevulinic acid (Merk), 0.4 g/L ^{12}glucose (VWR) as carbon source and 0.2 g/L $^{15}NH_4Cl$ (Cambridge Isotope Laboratories, Inc.) as nitrogen source. Then, the cultures were incubated at 30 ºC and 180 rpm, during 1h. Protein expression was induced with 100 µM IPTG. After induction, both unlabeled and labeled protein expression protocols remain the same.

3.1.2 Protein purification

The expressed ^{15}N isotopic labelled cytochrome PpcE was purified with resource of the same methods used for PpcF *G. metallireducens* purification (see section 2.1.2). However dialysis was made in 10 mM Tris-HCl pH 8.5 and cation exchange chromatography also in 10 mM Tris-HCl pH 8.5. Protein purity was evaluated by sodium dodecyl sulfate polyacrylamide gel electrophoresis (15%), stained with Coomassie brilliant blue (Sigma).

3.1.3 Protein expression yield

To the determination of the yield of the expressed cytochrome, the UV-visible spectra of PpcE in the reduced form was obtained using the same steps described is section 2.1.3. The PpcE concentration was determined by measuring the absorbance of the reduced PpcE α-band at 552 nm, using the extinction coefficient of 97.4 $mM^{-1}cm^{-1}$ determined for PpcA from *G. sulfurreducens* [36].

3.1.4 NMR studies

All the NMR experiments were acquired at pH 7 and 25 °C in a Bruker Avance III 600 MHz spectrometer equipped with a triple-ressonance cryoprobe. The water signal (4.81 ppm at 25 °C) was used to calibrate the ^{1}H chemical shifts and the ^{13}C and ^{15}N shifts calibrated through indirect referencing [39]. The obtained spectra were processed using software TOPSPIN (Bruker Biospin, Karlsruhe, Germany) and analyzed with program Sparky (TD Goddard and DG Kneller, Sparky 3, University of California, San Francisco, USA) and all the 1D-^{1}H NMR spectra referred in this work were acquired by collecting at 64k and at least 64 scans.

The backbone NH and heme methyl signals were previously assigned for PpcA [38, 39, 42]. Heme assignment were also assigned for PpcB and PpcE [50]. In the present work, the backbone signals for PpcB and PpcE were assigned using the methodology described in section 3.1.4.2.

3.1.4.1 Determination of interacting sites

The effect of the Fe(III) citrate addition was analyzed both on the backbone NH and on the heme methyl proton NMR signals using ^{15}N-labeled and natural abundance samples, respectively. Labeled cytochrome samples (0.5 mM) were prepared in 45 mM sodium phosphate buffer pH 7 with NaCl (100mM final ionic strength) in 92%H_2O/8% $^{2}H_2O$. The natural abundance samples were prepared in the same buffer but containing only pure $^{2}H_2O$.

Fe(III) citrate solution was prepared in 45 mM sodium phosphate buffer pH 7 with NaCl (100mM final ionic strength) and consecutive additions of 5M NaOH were made until the solution reach pH 7.

The effect of Fe(III) citrate on the backbone NH signals was monitored by the analysis of a series of 2D-^{1}H,^{15}N HSQC NMR spectra acquired for ^{15}N-labelled samples in the presence of increasing amounts of Fe(III) citrate in the following ratios of cytochrome:Fe(III) citrate: 1:0, 1:0.5, 1:1, 1:1.5, 1:2 and 1:3. The same experimental conditions were used to monitor the effect of Fe(III) citrate on the heme methyl signals via 2D-^{1}H,^{13}C HMQC (spectral width of 37 kHz in F_2 and 250 kHz in F_1)and 2D-^{1}H NOESY (spectral width of 37 kHz, mixing time of 80 ms) NMR spectra acquired with natural abundance samples. The pH of each cytochrome sample was measured before and after each series to confirm that pH of the solution is maintained. 1D-^{1}H NMR spectra were obtained before and after each 2D spectrum to confirm protein integrity.

3.1.4.2 NH backbone signals assignment methodology

The 2D-^{1}H,^{15}N HSQC spectra is the one where the magnetization is transferred from the ^{1}HN atom to the attached ^{15}N atom, via the J-coupling (Figure 17). In this type of spectra is possible to identify the N-H correlations of the sample, as well as the NH groups of the lateral chains of the residues (Appendix 3) such as Trp, His, Asn and Gln. This spectra constitutes a fingerprint of the sample.

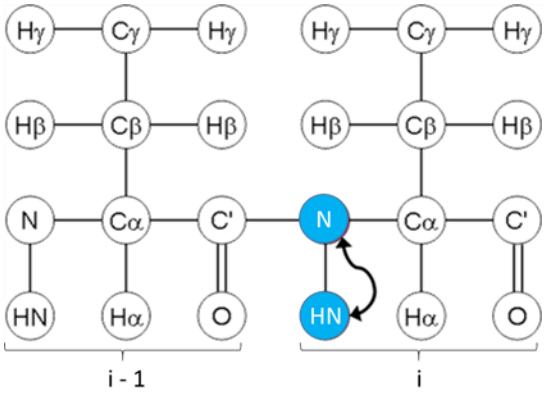

Figure 17. Scheme representing magnetization transfer in HSQC NMR experiment. In the HSQC experiment the magnetization (black arrow) is transferred from the hydrogen to the ^{15}N nuclei, as represented. Then, the magnetization is transferred back to the hydrogen for detection.

The quickest and safe way to assign the signals corresponding to the NH groups in the 2D-^{1}H,^{15}N HSQC spectra is to acquire a set of four experiences designated: 3D-HNCA, 3D-HNCACB, 3D-HN(CO)CA and 3D-HN(CO)CACB.

In a HNCA experiment, at first, the magnetization is passed from ^{1}HN to ^{15}N and then, via N-C_{α} J-coupling, to the $^{13}C_{\alpha}$. Then, the magnetization is passed back to ^{15}N and ^{1}HN respectively, therefore the signal is finally detected (Figure 18A). The chemical shift is evolved for ^{1}HN as well as the ^{15}N and $^{13}C_{\alpha}$, resulting in a three dimensional spectrum. Since the amide nitrogen is coupled to the C_{α} of its residue ($C_{\alpha i}$) and that of the preceding residue ($C_{\alpha i-1}$), both these transfers occur and the signals for both C_{α} are visible in the spectrum.

In the HN(CO)CA experiment we can visualize a single signal for each amino acid, corresponding to the $C_{\alpha i-1}$. In this particular experiment, the magnetization is passed from ^{1}HN to ^{15}N and then to the ^{13}C from the carbonyl group of the peptide bond. From there, the magnetization is transferred to $^{13}C_{\alpha}$ and the chemical shift is evolved. The magnetization is then transferred back, via ^{13}CO (the carbon from the carbonyl group of the peptide bond), to ^{15}N and ^{1}HN for detection (Figure 18B). The chemical shift is only evolved for the ^{1}HN, ^{15}N and $^{13}C_{\alpha}$, but not for the ^{13}CO. This results in a spectrum with similar results to the HNCA, being selective for the $C_{\alpha i-1}$.

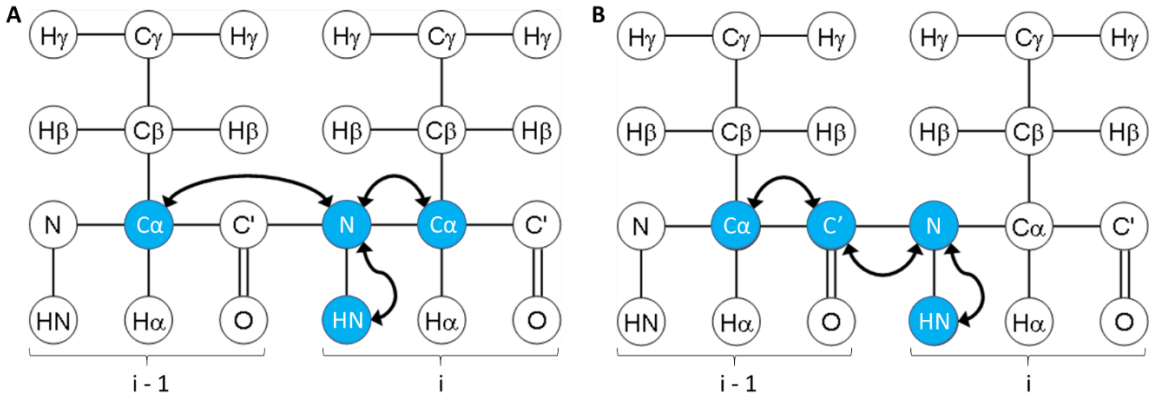

Figure 18. Schemes representing magnetization transfer in HNCA and HN(CO)CA NMR experiments. (A) HNCA experiment. The magnetization (black arrows) is transferred from the ^{1}H to ^{15}N and then, via N-C_{α} J-coupling, to the $^{13}C_{\alpha}$. Then, the magnetization is transferred back to ^{15}N and ^{1}H respectively, therefore the signal is finally detected. (B) HN(CO)CA experiment. The magnetization (black arrows) is passed from ^{1}H to ^{15}N and then to the ^{13}C from the carbonyl group of the peptide bond. From there, the magnetization is transferred to $^{13}C_{\alpha}$ and the chemical shift is evolved. The magnetization is then transferred back, via ^{13}CO (the carbon from the carbonyl group of the peptide bond), to ^{15}N and ^{1}H for detection. The chemical shift is only evolved for the ^{1}H, ^{15}N and $^{13}C_{\alpha}$, but not for the ^{13}CO. This results in a spectrum with similar results to the HNCA, being selective for the C_{α} of the preceding residue.

The HNCACB experience is less sensitive (low signal-to-noise ratio) and is generally used as a complementary way to verify the signals, especially the C_β from each ^1H,^{15}N HSQC signal. On a HNCACB experiment, the magnetization is transferred from $^1H_\alpha$ and $^1H_\beta$ to $^{13}C_\alpha$ and $^{13}C_\beta$, respectively, and then from $^{13}C_\beta$ to $^{13}C_\alpha$. From here it is transferred first to ^{15}N and then to ^1HN for detection. The transfer from $C_{\alpha i-1}$ can occur both to $^{15}N_{i-1}$ and $^{15}N_i$ or, viewed the other way, magnetization is transferred to $^{15}N_i$ from both $^{13}C_{\alpha i}$ and $^{13}C_{\alpha i-1}$ (Figure 19A). Thus, for each NH group there are two C_α and C_β peaks visible. The chemical shift is evolved simultaneously on $^{13}C_\alpha$ and $^{13}C_\beta$, therefore these appear in one dimension. The chemical shifts evolved in the other two dimensions are ^{15}N and ^1HN.

In the HN(CO)CACB experiment, both ^{13}C from the previous amino acid are visualized ($C_{\alpha i-1}$ and $C_{\beta i-1}$). This experiment also has a low signal-to-noise ratio. In this particular experiment (Figure 19B), the magnetization is transferred from $^1H_\alpha$ and $^1H_\beta$ to $^{13}C_\alpha$ and $^{13}C_\beta$, respectively, and then from $^{13}C_\beta$ to $^{13}C_\alpha$. From here it is transferred, at first, to ^{13}CO, then to ^{15}N and, finally, to ^1H for detection. The chemical shift is evolved simultaneously on $^{13}C_\alpha$ and $^{13}C_\beta$, therefore both appear in one dimension. The chemical shifts evolved in the other two dimensions are ^{15}N and ^1H. The chemical shift is not evolved on ^{13}CO.

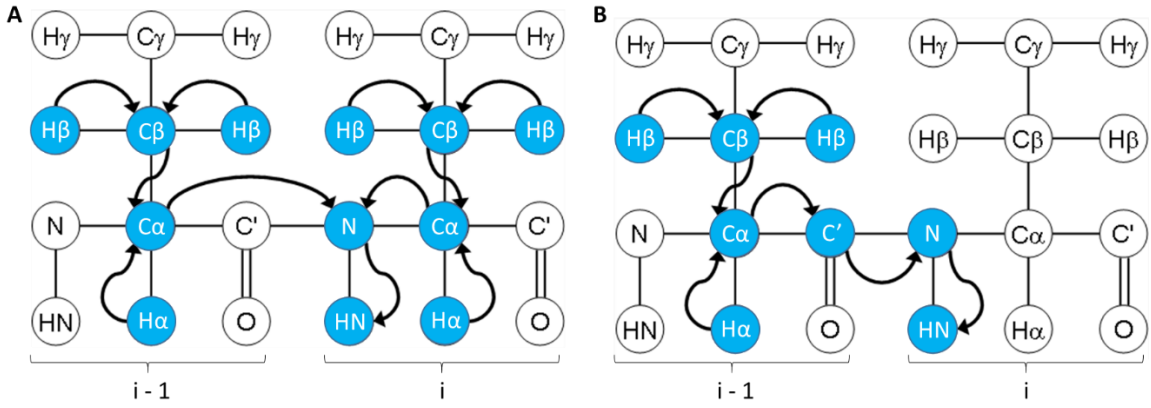

Figure 19. Schemes representing magnetization transfer in HNCACB and HN(CO)CACB NMR experiments. (A) HNCACB experiment. The magnetization (black arrows) is transferred from $^1H_\alpha$ and $^1H_\beta$ to $^{13}C_\alpha$ and $^{13}C_\beta$, respectively, and then from $^{13}C_\beta$ to $^{13}C_\alpha$. From here it is transferred first to ^{15}N and then to ^1H for detection. The transfer from $^{13}C_{\alpha i-1}$ can occur both to $^{15}N_{i-1}$ and $^{15}N_i$ or, viewed the other way, magnetization is transferred to $^{15}N_i$ from both $^{13}C_{\alpha i}$ and $^{13}C_{\alpha i-1}$. The chemical shift is evolved simultaneously on $^{13}C_\alpha$ and $^{13}C_\beta$, therefore these appear in one dimension (B) HN(CO)CACB experiment. The magnetization (black arrows) is transferred from $^1H_\alpha$ and $^1H_\beta$ to $^{13}C_\alpha$ and $^{13}C_\beta$, respectively, and then from $^{13}C_\beta$ to $^{13}C_\alpha$. From here it is transferred, at first, to ^{13}CO, then to ^{15}N and, finally, to ^1H for detection.

In the protein assignment, at first, a random signal from the general HSQC spectrum was chosen, and using the ^{15}N and ^{13}C chemical shifts, its path was followed into the 3D spectra. All the 3D spectra recorded were aligned with the HSQC and between themselves, so that all ^{15}N, ^{13}C and ^{1}H chemical shifts variations could be followed simultaneously. For the assignment of the C_α of each amino acid, the HNCA spectra were used to find the $C_{\alpha i}$ and $C_{\alpha i-1}$ chemical shifts, and to distinguish between them, the HNCOCA was used, since only the $C_{\alpha i-1}$ appears in this spectrum. This assignment can be also confirmed in the HNCACB and HNCOCACB. At the same time, for the assignment of the C_β, the HNCACB spectra were used to find the C_β and $C_{\beta i-1}$ chemical shifts, and to distinguish between them, the HNCOCACB was used, since only the $C_{\beta i-1}$ appears in this spectrum. After getting all the possible information from a single HSQC signal, we then navigated either to its following amino acid or to its previous one. In order to navigate to any following amino acid, we used the HNCOCA spectra and by fixing the $C_{\alpha i}$, and varying the ^{15}N dimension, it was possible to find correspondent peaks (peaks with similar ^{13}C chemical shift, but different ^{15}N and ^{1}H chemical shift). This new signals corresponded to an amino acid, placed on the right from the one we started from. That means that the signals founded were actually the C_α from the first amino acid being seen as a previous C_α.

A similar strategy can be followed in order to navigate to any previous amino acid. For that, we used the HNCA spectra and fixed the chemical shift of $C_{\alpha i-1}$. The new signals founded corresponded to the previous amino acid itself, meaning that the C_α previously seen as a $C_{\alpha i-1}$, was now seen as a C_α belonging to the amino acid itself.

By continuously using the method above described (peaking a HSQC peak, and navigate to its previous and following amino acids), the assignment of the protein backbone was obtained (Figure 20).

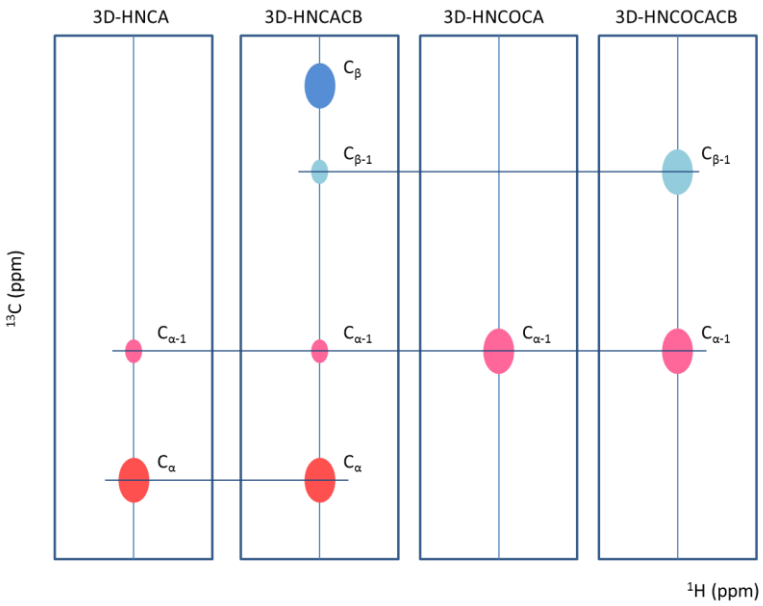

Figure 20. Scheme of the observable signals in 3D-HNCA, 3D-HNCACB, 3D-HNCOCA and 3D-HNCOCACB NMR spectra in ^{1}H and ^{13}C coordinates for a given ^{15}N chemical shift.

3.2.1 Protein expression

After the isolation of the periplasmic fraction, the expressed ^{15}N PpcE from *G. sulfurreducens* was purified by cation exchange and molecular exclusion chromatography. The elution profiles obtained from both chromatographic methods are shown in Figures 21 and 22, respectively.

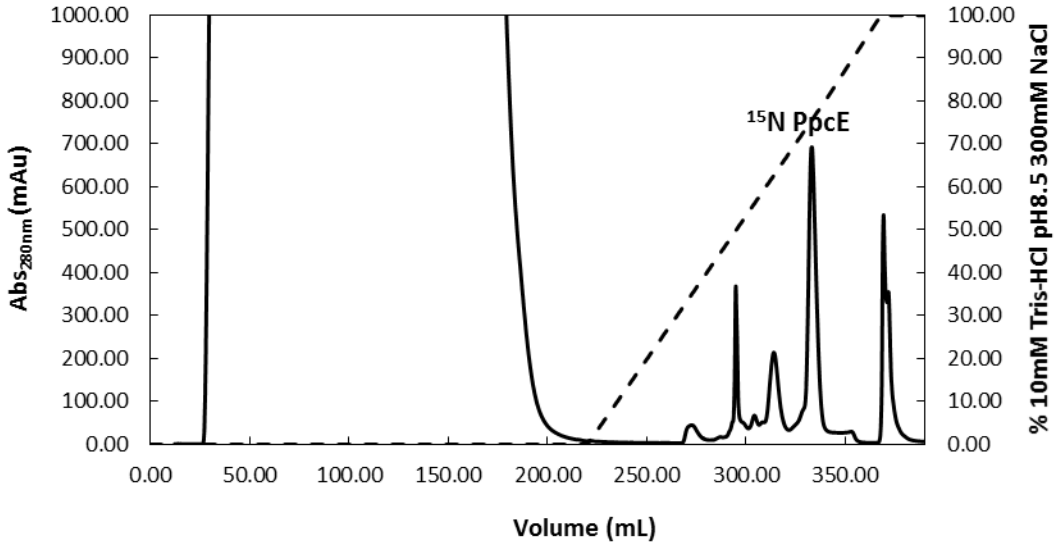

Figure 21. Elution profile for the cation exchange chromatography of PpcE from *G. sulfurreducens*. Cation exchange chromatography column equilibrated with 10 mM Tris-HCl pH 8.5. Elution at 1 mL/min flow rate. Solid line corresponds to the variation of absorbance at 280 nm. Dashed line reports the NaCl gradient profile.

Based on the amino acid sequence of PpcE an isoelectric point of 9.51 was determined using the pI/Mw tool program on the ExPASy Server. Considering this, PpcE was purified using a cation exchange column equilibrated with 10 mM Tris-HCl pH 8.5. The elution of the cytochrome and other column-bound proteins were achieved by increasing the buffer ionic strength. The bound proteins are eluted with a sodium chloride gradient of 150 mL, between 0 and 300 mM. The protein of interest, which presents a red characteristic color, typical for proteins containing heme groups, was eluted at 75% (225 mM) of the gradient, as depicted in Figure 21.

This purification step allowed the removal of the bulk of the contaminants and the remaining ones were removed by a molecular exclusion chromatography step, whose chromatogram is

indicated in Figure 22. The molecular weight of PpcE is 9661 Da (theoretical value determined with *Compute pI/Mw tool* [46] and was eluted at 93 mL, with 100 mM sodium phosphate buffer (pH 8).

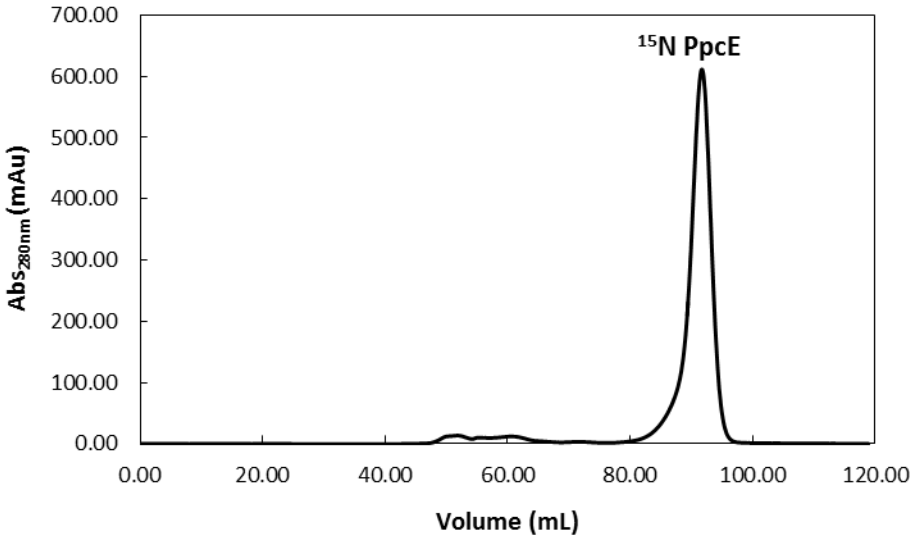

Figure 22. Elution profile for the molecular exclusion chromatography of PpcE from *G. sulfurreducens*. Molecular exclusion chromatography column equilibrated with 100 mM sodium phosphate buffer, pH 8, with a flow rate of 0.5 mL/min.

The purity of PpcE was accessed by SDS-PAGE electrophoresis (Figure 23). The analysis of the resulting gel shows a single intense band at approximately 10 kDa, which agrees with the actual molecular weight of the cytochrome. The protein yield was 1.31 mg per liter of cell culture determined as described in section 3.1.3.

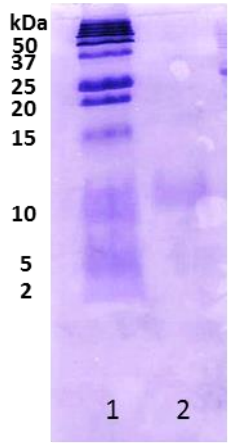

Figure 23. Purity analysis by SDS-PAG electrophoresis of PpcE from *G. sulfurreducens*. Obtained results of SDS-PAGE gel, 15% acrylamide, stained with Coomassie brilliant blue. Lane 1) Purified fraction after molecular exclusion chromatography; Lane 2) Protein marker (Protein Plus Protein Dual Xtra Standards, Bio-Rad, appendix 1); The molecular weights of the protein markers are in indicated on the left of lane 1.

3.2.2 NH backbone signals assignment of PpcB and PpcE

As previously mentioned, the NH backbone signals of PpcA (Figure 24) have been previously assigned [54]. The NH signals of PpcB and PpcE were assigned in the present work (Figure 24) as described in section 3.1.4.2, except for Ala^{1}, Asp^{2}, Gly^{42} and Cys^{51} for PpcB and Ala^{1}, Asp^{2}, Gly^{42} and Thr^{62} for PpcE. The backbone NH signals at the N-terminal residues (Ala^{1}, Asp^{2}) are usually not observable due to fast exchange. The backbone NH signal of Gly^{42} were not observable, most probably due to signal broadening caused by the nearby hemes I and IV paramagnetic irons. This signal was also not observable in PpcA. Therefore, taking into consideration the similar location of this residue in PpcA and the other members of the PpcA family from *G. sulfurreducens* (Figure 3) the proximity to the paramagnetic centers is also probably the explanation for the excessive line broadening of the NH signal of Gly^{42}. On the other hand, the backbone amide signals of Cys^{51} and Thr^{62} were not observed most probably due to their rapid solvent exchange at pH 7.

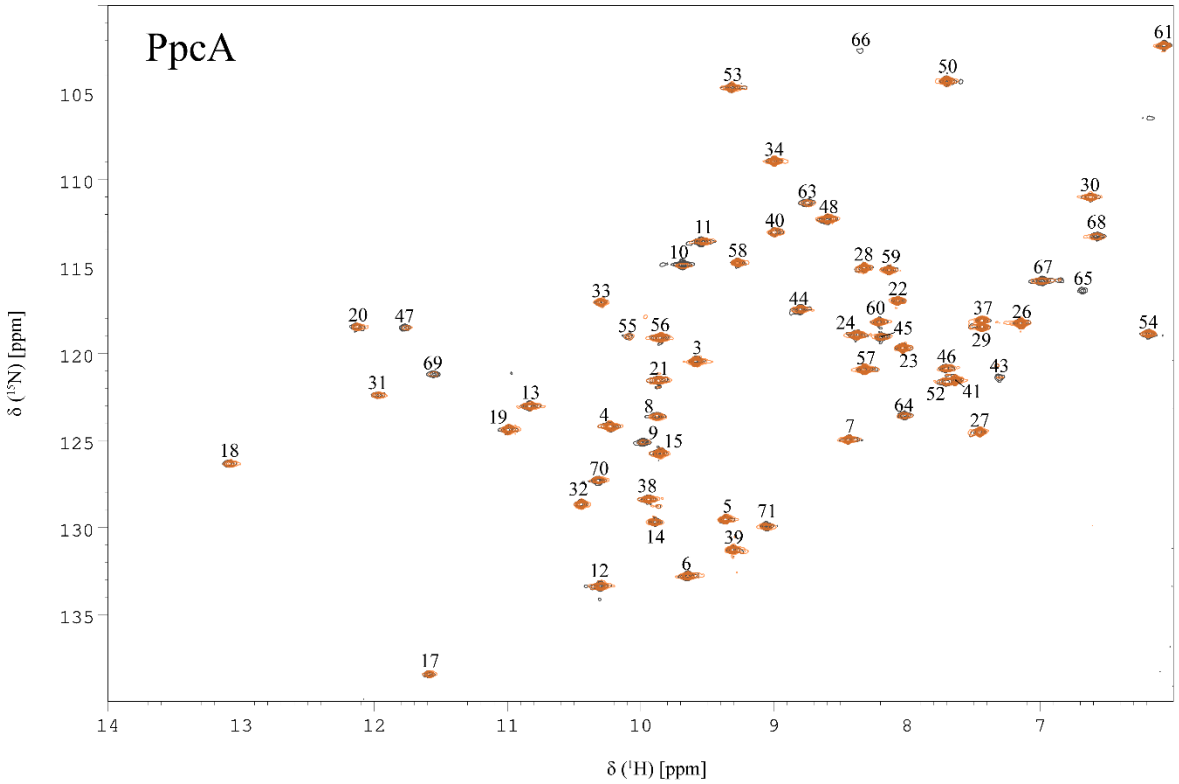
PpcA
δ (15N) [ppm]
δ (1H) [ppm]

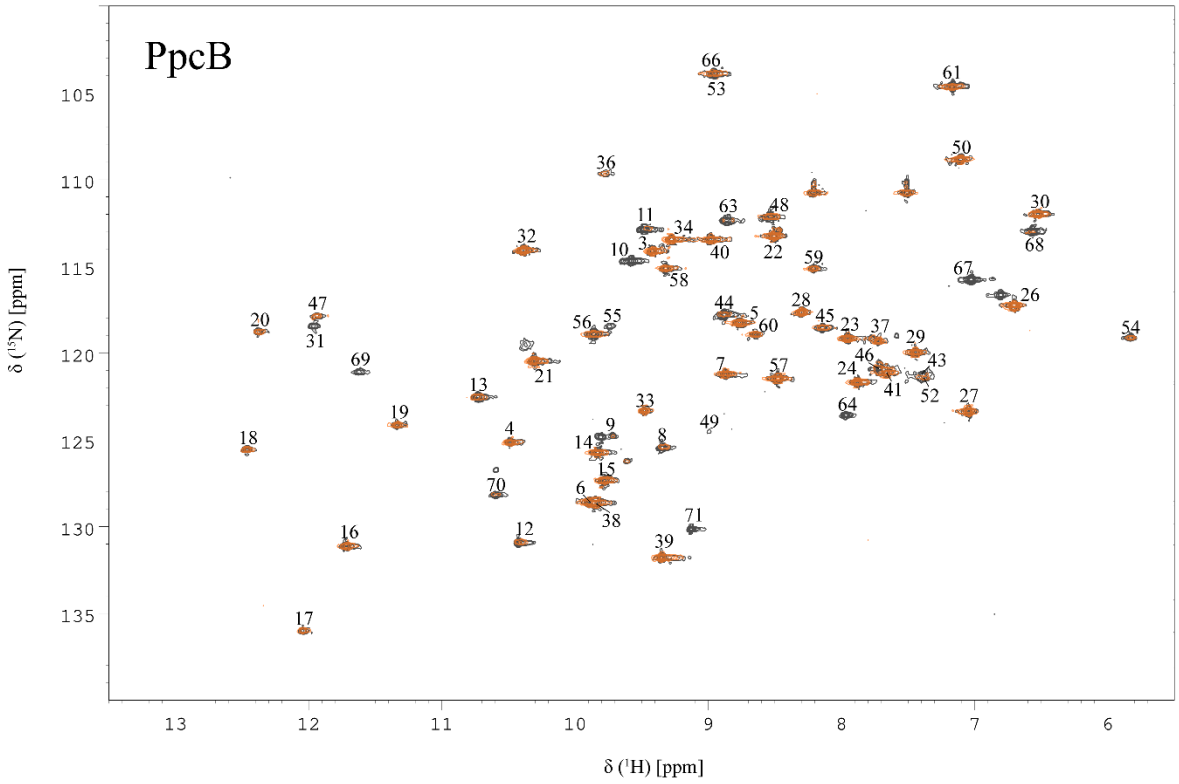
PpcB
δ (15N) [ppm]
δ (1H) [ppm]

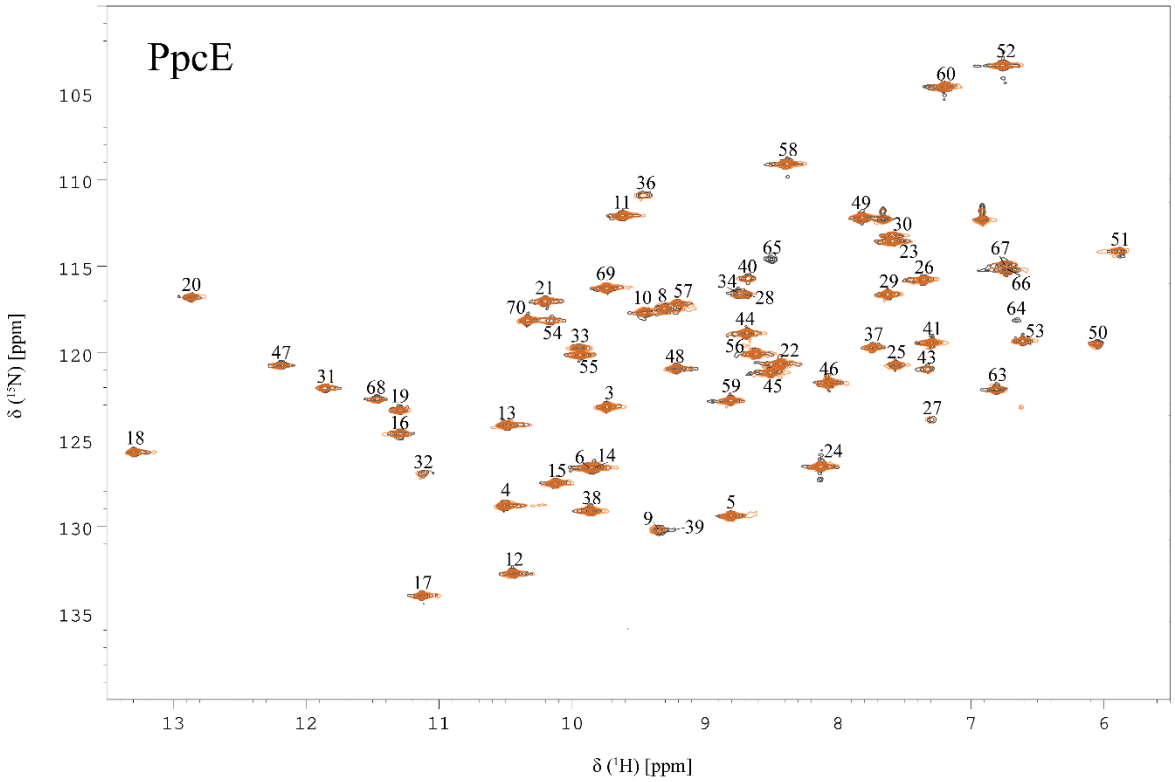

Figure 24. Overlay of the 2D-^{1}H,^{15}N HSQC NMR spectra of ^{15}N-enriched PpcA, PpcB and PpcE samples obtained in the absence and in the presence of Fe(III) citrate. The contours of the signals in the absence and in the presence of Fe(III) citrate are indicated in black and orange, respectively. The assignments of NH signals are indicated.

3.2.3 Interaction between the triheme cytochromes PpcA, PpcB and PpE and Fe(III) citrate

The effect of the addition of increasing amounts of Fe(III) citrate on the backbone NH signals of the cytochromes were monitored by recording a series of 2D-^{1}H,^{15}N HSQC NMR spectra. Figure 25 exhibits a partial area of the spectra obtained for each cytochrome in the absence and in presence of Fe(III) citrate in a ratio 1:3, whereas the full spectra are indicated in Figure 24. Sensible line broadening is observed upon addition of Fe(III) citrate to the cytochromes. In the case of PpcA, the residues whose amide resonances showed a decrease in the peak data height loss above 80% are placed in polypeptide segments Lys^{9}-Gly^{11} and Lys^{64}-His^{69}, as well as residues Glu^{44} and Lys^{71}. All the most affected residues in PpcA are located near heme IV. For PpcB the most affected residues are Ala^{8}-Val^{13}, His^{31}, Lys^{43}-Ala^{46}, Gly^{48}, Lys^{49}, Lys^{52}, Gly^{53}, Glu^{56}, Thr^{63}-Lys^{71}. As in the case of PpcA, in PpcB the most affected residues are also located near heme IV, except residue His^{31} that is near heme I. Finally, the residues that showed considerably line width broadening upon addition of Fe(III) citrate

in PpcE are located in the polypeptide segment Lys^{63}- Leu^{66}, which is also placed at the vicinity of heme IV. The analysis of the line width broadening on the backbone NH and heme methyl signals of each cytochrome enabled us to map the interaction region in each Fe(III)-citrate:cytochrome redox-complex. The observed increase in the line width broadening, as a function of Fe(III) citrate concentration, is attributable to the presence of the iron ion in the Fe(III) citrate molecule. In fact, Fe(III) is a d^3 ion, generally six-coordinated, with three unpaired electrons (S=3/2). It possesses negligible magnetic anisotropy and, therefore does not contribute to the hyperfine shifts of neighbor nuclei. Instead it broadens the NMR lines because of its short electronic relaxation times.

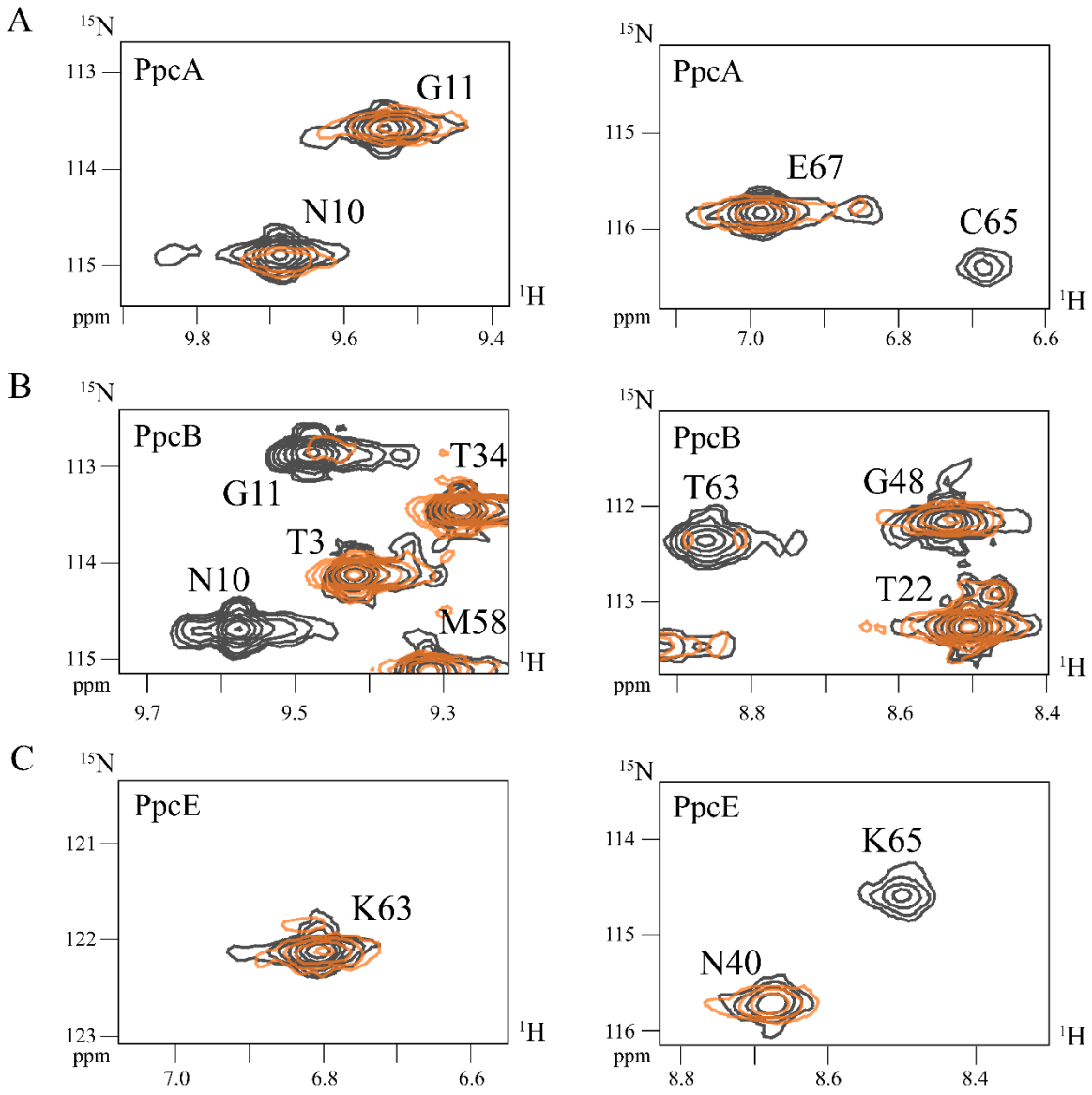

Figure 25. Selected spectral regions of 2D-^{1}H,^{15}N HSQC NMR spectra acquired for ^{15}N-enriched PpcA (A), PpcB (B) and PpcE (C) in the absence and in the presence of Fe(III) citrate. Full spectra are indicated in Figure 24. The assignments of NH signals are indicated.

The residues experiencing significant line width broadening upon addition of Fe(III) citrate in the three cytochromes are highlighted on the three-dimensional structure of the proteins (Figure 26). In all cytochromes, the most affected residues are located in polypeptide regions that enwrap heme IV. The location of the complex interface in a similar region in all cytochromes is not surprising since the three proteins have high sequence and structural homology [34].

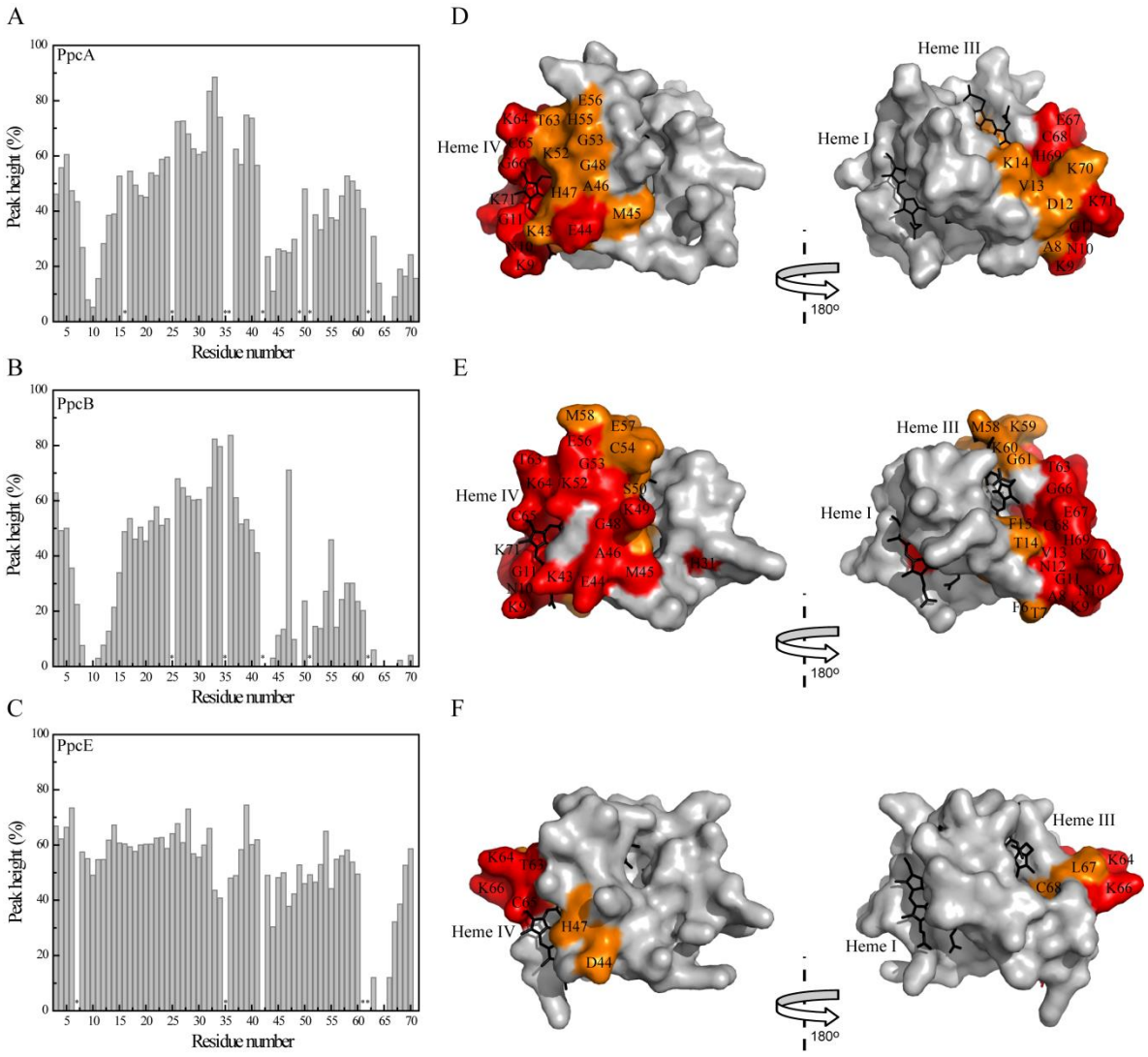

Figure 26. Line width broadening effects on the PpcA, PpcB and PpcE backbone NH signals and respective surface mapping. The peak height of the signals (%) measured for each cytochrome in the presence of Fe(III) citrate (1:3 ratio) is indicated in the left handed panels (A) PpcA; (B) PpcB and (C) PpcE). Asterisks indicate proline or non-assigned residues. Residues whose signals showed a decrease in the peak data height loss in the range 100% - 80% and 80% - 60% are represented in red and orange, respectively in the corresponding right-handed panels (D) PpcA; (E) PpcB and (F) PpcE). In each surface map the hemes are shown in black. The molecular surface was generated in PyMOL [40] by using structures of PpcA (PDB code, 2LDO [32]), PpcB (PDB code, 3BXU [33]) and PpcE (PDB code, 3H34 [34]).

Owing the reduction potentials of the heme groups of PpcA, PpcB and PpcE (Table 1) and that of Fe(III) citrate (+ 372 mV *versus* SHE [55]) the reduction of the latter is clearly thermodynamically favorable and can be achieved via any of the hemes. Moreover, to the electron transfer occur at physiologically relevant rates between each cytochrome and Fe(III) citrate at least one heme group

and the acceptor must be in close proximity to warrant for an effective electron transfer. If this is the case, any perturbation caused by binding of Fe(III) citrate is expected to affect the NMR signals of the heme substituents. In order to investigate this, we further study the effect of the addition of Fe(III) citrate on the heme methyl signals in each cytochrome.

Each heme has four methyl groups (2^1CH_3, 7^1CH_3, 12^1CH_3 and 18^1CH_3, see Figure 27) and their ^1H NMR signals are found typically in less crowded regions of the 1D-^1H NMR spectrum. For this reason, they constitute excellent probes for monitoring the effect of the addition of Fe(III) citrate on PpcA, PpcB and PpcE heme groups. The heme methyl signals of the cytochromes were previously assigned [47, 54] and both 1D-^1H and 2D-^1H NOESY NMR spectra were used to further evaluate the interactions between Fe(III) citrate and each protein. The low-field regions of the 1D-^1H NMR spectra, acquired during the titration of each cytochrome with increasing amounts of Fe(III) citrate are indicated in Figure 27. In this spectral window 11 out of 12 heme methyls can be easily followed. The signal of the heme methyl $18^1CH_3^{III}$ appears at 0.76 ppm, 1.54 and -0.14 ppm, in PpcA, PpcB and PpcE, respectively and therefore cannot be easily probed by 1D-^1H NMR titrations. In order to evaluate the effect of the addition of Fe(III) citrate on the complete set of heme methyl signals, 2D-^1H,^{13}C HMQC NMR spectra were recorded for each cytochrome in the absence and in the presence of Fe(III) citrate (Figure 28A). The analysis of both 1D-^1H NMR titrations (Figure 27) and 2D-^1H,^{13}C HMQC NMR spectra obtained in the presence of Fe(III) citrate (Figure 28A) clearly shows that there is a dramatic increase in the line width of the heme IV methyl signals. Another strong evidence that further confirms the complex interface in this region is provided by the significant line width broadening observed for heme IV methyl signals, whereas those from hemes I and III are essentially unaffected with the increasing addition of Fe(III) citrate (Figure 27). Interestingly, the most solvent-exposed methyl groups of heme IV ($2^1CH_3^{IV}$ and $18^1CH_3^{IV}$) clearly show a more pronounced effect than the other methyl groups of heme IV ($7^1CH_3^{IV}$ and $12^1CH_3^{IV}$), which are buried in the protein core. The effect becomes more evident as the titration progresses (Figure 27). Heme IV methyls $2^1CH_3^{IV}$ and $18^1CH_3^{IV}$ are clearly the most affected ones compared with $7^1CH_3^{IV}$ and $12^1CH_3^{IV}$. All the other heme resonances remained essentially unchanged in terms of line width broadening. These observations were further confirmed by analysis of the heme methyl NOE connectivities in the 2D-^1H NOESY NMR spectra obtained for each cytochrome in the absence and in the presence of Fe(III) citrate (Figure 28B). In fact, only the heme IV methyls, in particular ($2^1CH_3^{IV}$ and $18^1CH_3^{IV}$) showed considerable decrease in the NOE connectivities, as a result of the significant line width broadening of their signals in the presence of Fe(III) citrate. Overall, the line width broadening on the heme IV

methyl signals reinforces the observation that there is binding of Fe(III) citrate to each cytochrome near this heme.

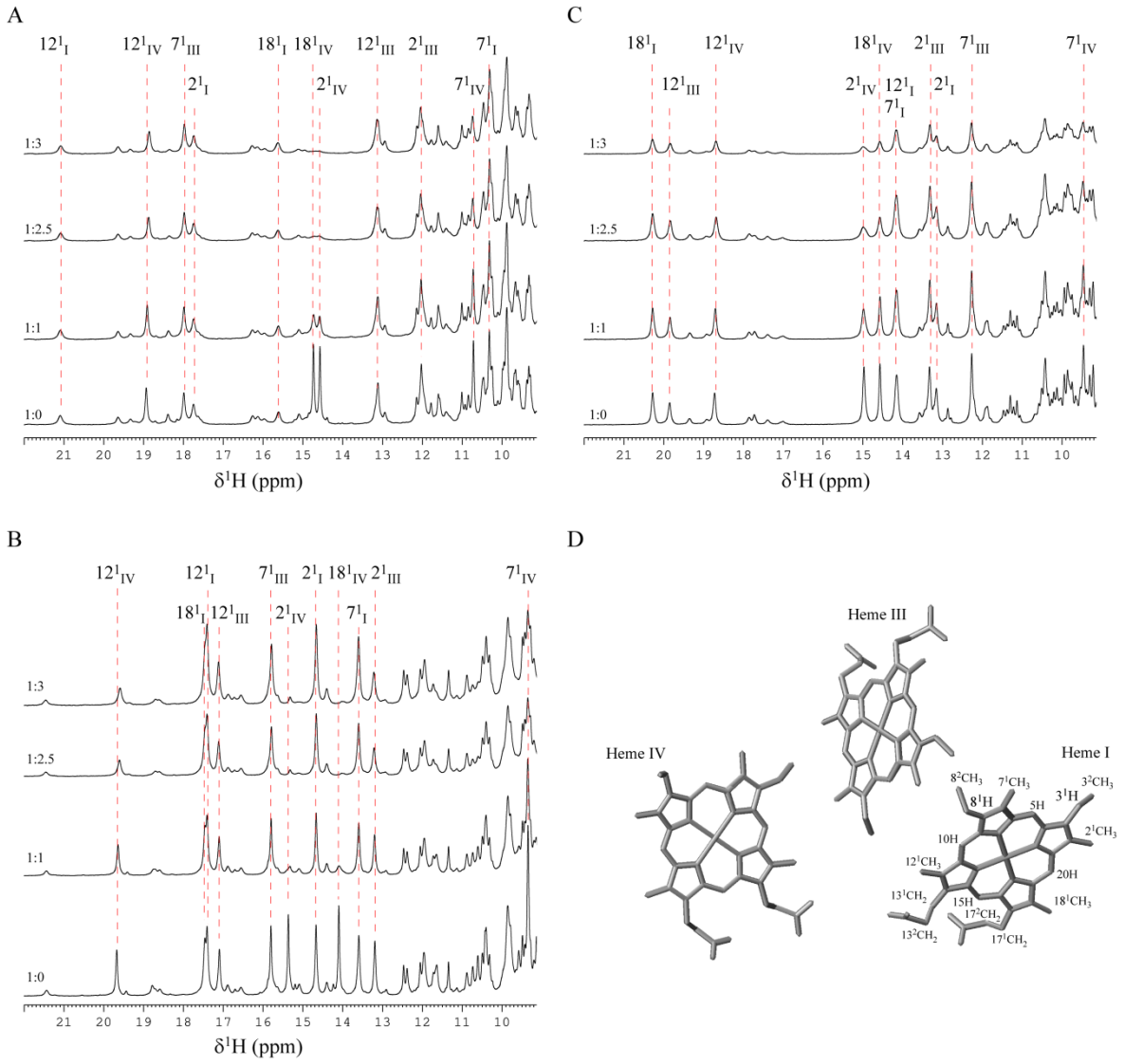

Figure 27. Line broadening effects on heme methyl ^{1}H signals of PpcA, PpcB and PpcE cytochromes. Expansions of the low-field region of 1D-^{1}H NMR spectra obtained for PpcA, PpcB and PpcE in presence of increasing amounts of Fe(III) citrate: (A) PpcA, (B) PpcB and (C) PpcE. The heme methyl signals ($2^{1}CH_3$, $7^{1}CH_3$, $12^{1}CH_3$ and $18^{1}CH_3$) following the IUPAC nomenclature [39] are labeled, with exception of heme methyl $18^{1}CH_3{}^{III}$ whose signal appears at a chemical shift of approximately 1 ppm (see Figure 28). The protein:Fe(III) citrate ratio used in each experiment is indicated on the left of each spectrum. D) The heme core architecture of the cytochromes is illustrated by that of PpcA (PDB code 2LDO, [32]). The IUPAC nomenclature for tetrapyrroles [29] is illustrated in heme I.

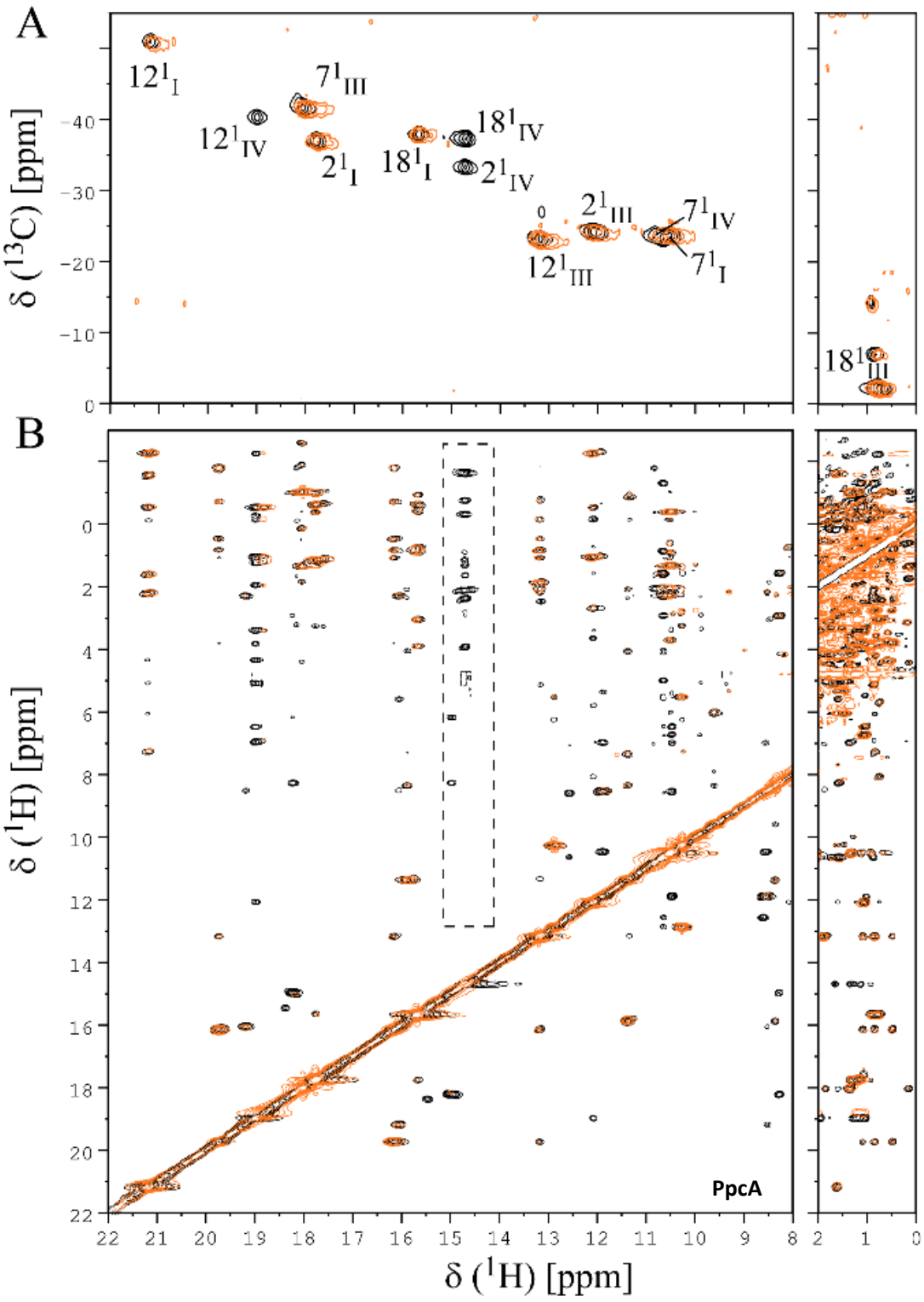
A
B
12^1_I
7^1_{III}
12^1_{IV}
18^1_{IV}
2^1_I
18^1_I
2^1_{IV}
2^1_{III}
7^1_{IV}
12^1_{III}
7^1_I
18^1_{III}
PpcA
δ (^{13}C) [ppm]
δ (^{1}H) [ppm]
δ (^{1}H) [ppm]

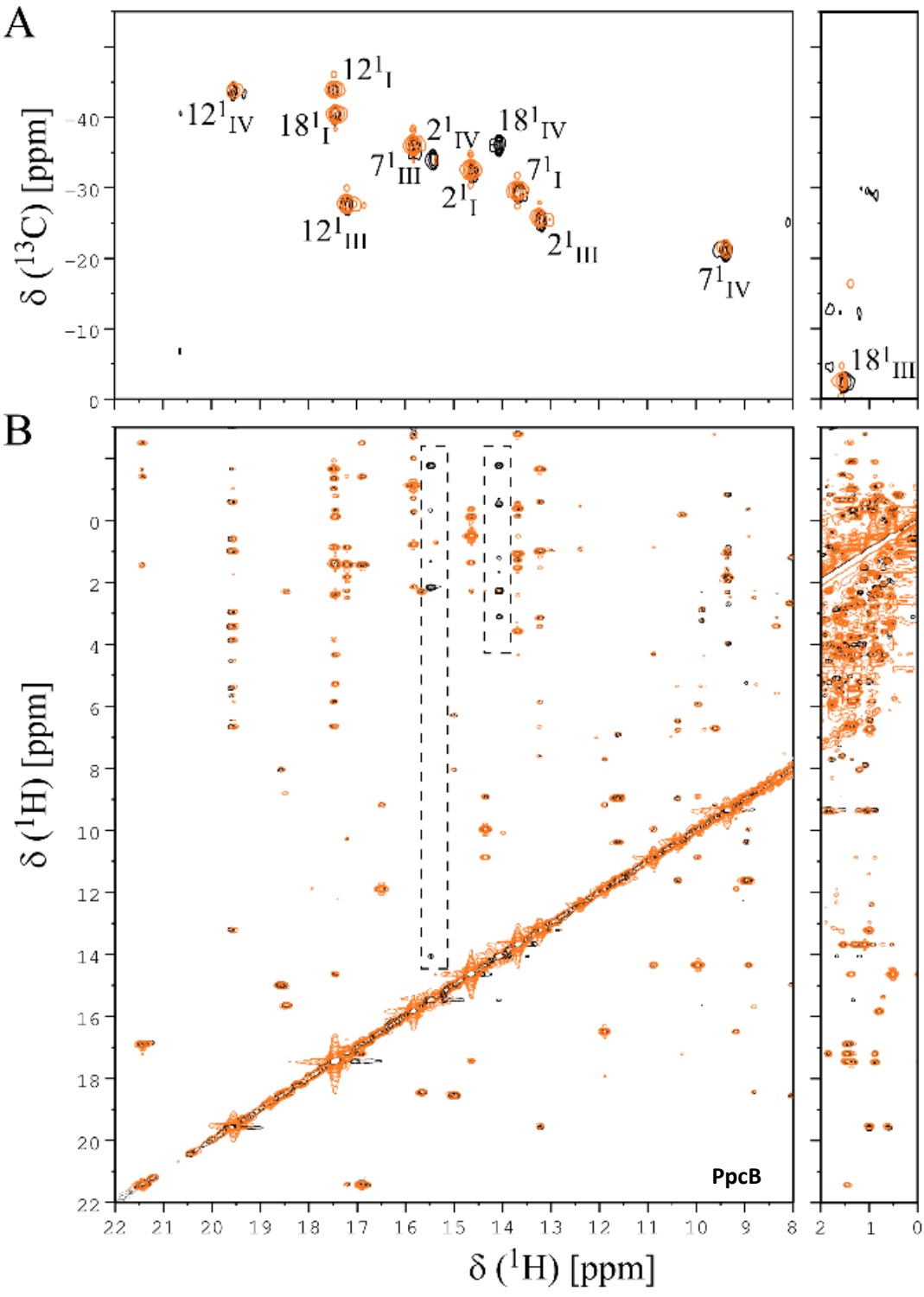
A
B
δ (13C) [ppm]
δ (1H) [ppm]
δ (1H) [ppm]
12 1 I
12 1 IV
18 1 I
2 1 IV
18 1 IV
7 1 III
7 1 I
2 1 I
12 1 III
2 1 III
7 1 IV
18 1 III
PpcB

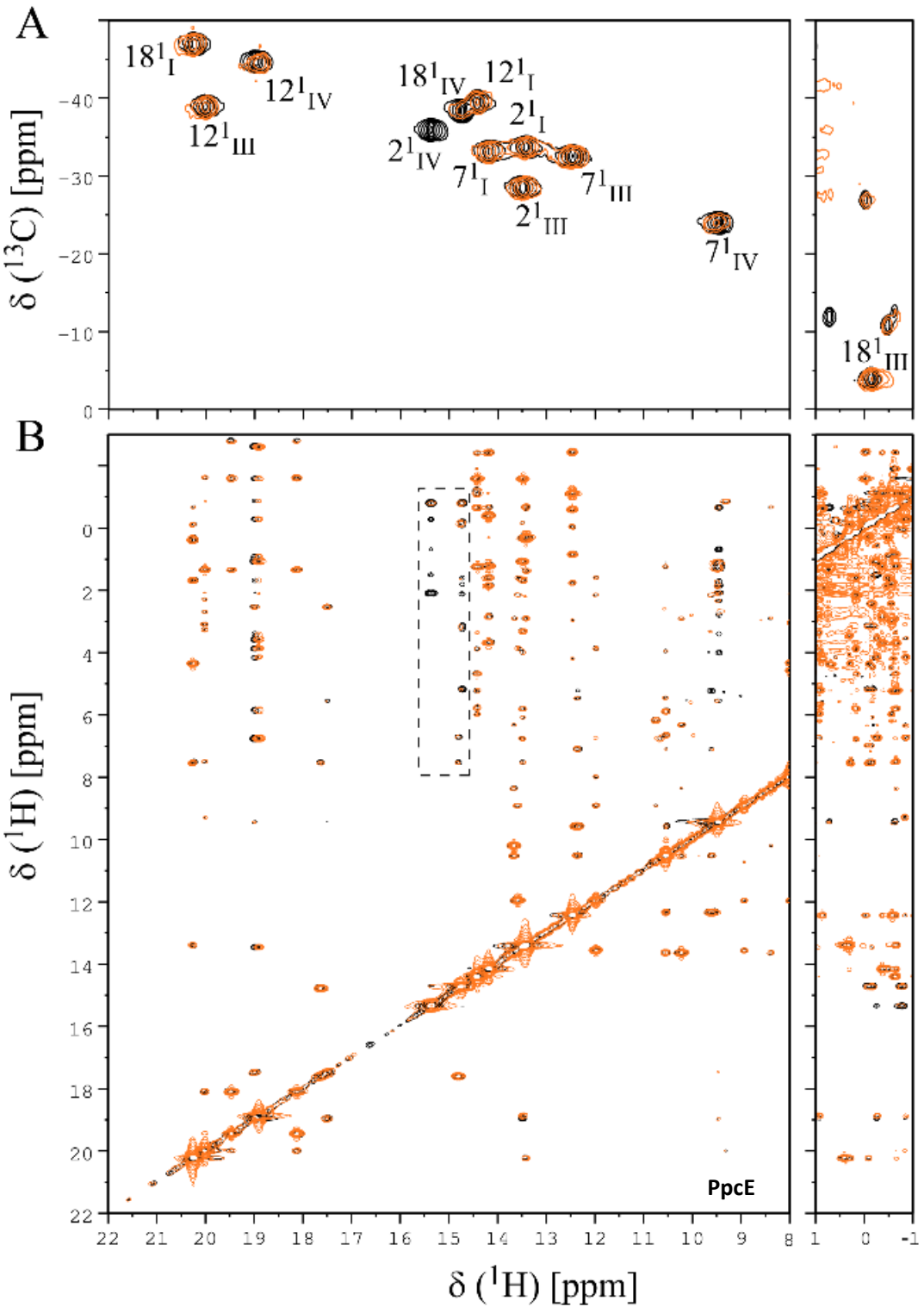

Figure 28. Selected regions of 2D-^{1}H,^{13}C HMQC (A) and 2D-^{1}H NOESY (B) NMR spectra of PpcA, PpcB and PpcE cytochromes in the absence (black) and presence (orange) of Fe(III) citrate. The dashed rectangles show the NOE connectivities of heme methyls $2^1CH_3^{IV}$ and $18^1CH_3^{IV}$ whose signals show significantly broadening upon addition of Fe(III) citrate.

The heme groups of each cytochrome are considerably exposed to the solvent, with heme I showing the largest exposure [43, 44]. Therefore, the selective interaction between Fe(III) citrate and the cytochromes in the region of heme IV must be driven by other factors than simple heme exposure. In fact, the analysis of the structures showed that the cytochromes have the highest degree of conservation around heme IV [34]. The protein surface around this heme is positively charged due to the presence of several lysine residues, thus all cytochromes could interact with similar molecules involving this region. Therefore, considering the net positive charge of the cytochromes around heme IV and the negative nature of Fe(III) citrate, electrostatic interactions are expected to contribute favorably to the formation of the cytochrome:Fe(III) citrate redox complexes. However, the detailed analysis of the residues experiencing significant line width broadening in the three cytochromes (see panels D-F in Figure 26) shows that in PpcE fewer residues experienced broadening compared to PpcA and PpcB, resulting in a less extensive interaction site and thus suggesting the formation of a more specific complex between Fe(III) citrate and PpcE. A possible explanation for this observation relies on the specific geometry of the two most affected lysine residues (Lys^{64} and Lys^{66}) in PpcE. In fact, the two lysine residues enwrapped Cys^{65} that forms the heme IV binding motif, a feature that is not observed in the other two cytochromes (Figure 29) and can be responsible for the specific driving of Fe(III) citrate to this region of PpcE.

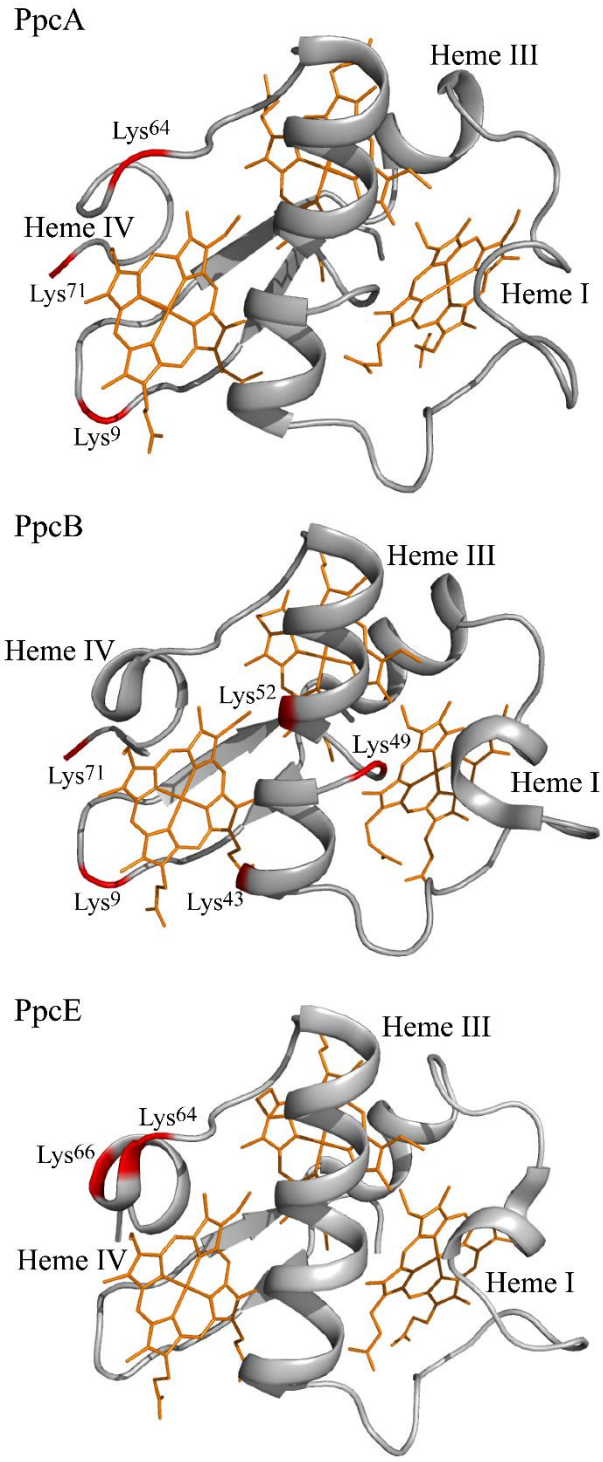

Figure 29. Structural map of the most affected lysine residues in PpcA, PpcB and PpcE in the presence of Fe(III) citrate. The images were generated in PyMOL [40] by using the structures of PpcA (PDB code: 2LDO [32]), PpcB (PDB code: 3BXU [33]) and PpcE (PDB code: 3H34 [34]).

3.3 CONCLUSIONS

In this work PpcE labelled in ^{15}N was heterologously expressed in *Escherichia coli* and purified with a yield of 1.31 mg per liter of cell culture. The NH backbone signals of this cytochrome, as well as those of PpcB were successfully assigned.

The study described in this chapter provides a clear picture of the molecular interaction between cytochromes PpcA, PpcB and PpcE with Fe(III) citrate. The results obtained constitute an important step toward the rationalization of the *G. sulfurreducens* iron compounds respiratory chains that utilize iron compounds as terminal electron acceptors, in particular those involved in the reduction of Fe(III) citrate. Previous structural and thermodynamic studies carried out on the three targeted cytochromes showed that the reduction potentials of the heme groups redox are negative covering the redox potential window of -100 to -158 mV [37]. Therefore, in a thermodynamic point of view, Fe(III) citrate can be putatively reduced by any heme group in each cytochrome. However, the NMR experiments carried out in the present study showed that this is not the case, as Fe(III) citrate binds to the three cytochromes in a well specific and defined patch containing positively charged lysine residues close to the more solvent-exposed heme IV methyl groups. The presence of positive residues in the vicinity of heme IV methyl groups promotes favorable electrostatic docking to each cytochrome. The present results obtained for Fe(III) citrate become quite relevant beyond the scope of periplasmic cytochromes and can be also used as working-models for the *Geobacter* outer membrane cytochromes for which structural data are still currently unavailable.

Chapter 4: Future perspectives

4. FUTURE PERSPECTIVES

The NMR and the partial thermodynamic characterization of PpcF performed in this work constitute the building blocks to determine the structure of this cytochrome, which is yet unknown. The data obtained will also allow a more detailed thermodynamic characterization that will include the determination of the microscopic potentials and the properties of the redox-Bohr center, as a first step to elucidate the extracellular electron transfer pathways in G. metallireducens. These pathways are slightly better understood in G. sulfurreducens and within this context, the work developed on chapter 3, that included the assignment of the backbone NH NMR signals of the periplasmic triheme cytochromes and the mapping of their interaction regions with the terminal electron acceptor Fe(III) citrate, constitutes an important foundation to assist in new interaction studies with different electron acceptors or redox partner proteins.

Chapter 5: References

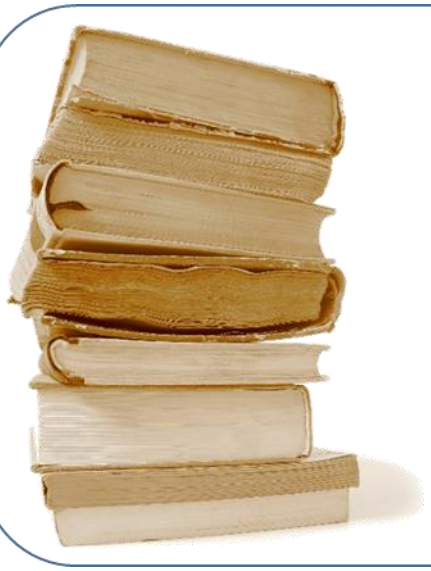

5. REFERENCES

[1] D. R. Lovley, T. Ueki, T. Zhang, N. S. Malvankar, P. M. Shrestha, K. A. Flanagan, M. Aklujkar, J. E. Butler, L. Giloteaux, A. E. Rotaru, D. E. Holmes, A. E. Franks, R. Orellana, C. Risso, and K. P. Nevin, *Geobacter*. The Microbe Electric's Physiology, Ecology, and Practical Applications, *Adv. Microb. Physiol.*, vol. 59, pp. 1–100, 2011.

[2] R. T. Anderson, H. A. Vrionis, I. Ortiz-bernad, C. T. Resch, P. E. Long, R. Dayvault, K. Karp, S. Marutzky, D. R. Metzler, A. Peacock, D. C. White, M. Lowe, and D. R. Lovley, Stimulating the In Situ Activity of *Geobacter* Species To Remove Uranium from the Groundwater of a Uranium-Contaminated Aquifer, *Appl. Environ. Microbiol.*, vol. 69, no. 10, pp. 5884–5891, 2003.

[3] K. B. Gregory and D. R. Lovley, Remediation and Recovery of Uranium from Contaminated Subsurface Environments with Electrodes, *Environ. Sci. Technol.*, vol. 39, no. 22, pp. 8943–8947, 2005.

[4] J. N. Rooney-Varga, R. T. Anderson, J. L. Fraga, D. Ringelberg, and D. R. Lovley, Microbial communities associated with anaerobic benzene degradation in a petroleum-contaminated aquifer, *Appl. Environ. Microbiol.*, vol. 65, no. 7, pp. 3056–3063, 1999.

[5] D. R. Lovley, D. E. Holmes, and K. P. Nevin, Dissimilatory Fe(III) and Mn(IV) reduction, *Advances in Microbial Physiology*, vol. 49. pp. 219–286, 2004.

[6] D. R. Lovley, Live wires: direct extracellular electron exchange for bioenergy and the bioremediation of energy-related contamination, *Energy Environ. Sci.*, vol. 4, no. 12, p. 4896, 2011.

[7] D. R. Lovley, Electromicrobiology, *Annu. Rev. Microbiol.*, vol. 66, no. 1, pp. 391–409, 2012.

[8] D. R. Bond and D. R. Lovley, Electricity production by *Geobacter sulfurreducens* attached to electrodes, *Appl. Environ. Microbiol.*, vol. 69, no. 3, pp. 1548–1555, 2003.

[9] K. P. Nevin, H. Richter, S. F. Covalla, J. P. Johnson, T. L. Woodard, A. L. Orloff, H. Jia, M. Zhang, and D. R. Lovley, Power output and columbic efficiencies from biofilms of *Geobacter sulfurreducens* comparable to mixed community microbial fuel cells, *Environ. Microbiol.*, vol. 10, no. 10, pp. 2505–2514, 2008.

[10] M. Izallalen, R. Mahadevan, A. Burgard, B. Postier, R. Didonato, J. Sun, C. H. Schilling, and D. R. Lovley, *Geobacter sulfurreducens* strain engineered for increased rates of respiration, *Metab. Eng.*, vol. 10, no. 5, pp. 267–275, 2008.

[11] B. a Methé, K. E. Nelson, J. a Eisen, I. T. Paulsen, W. Nelson, J. F. Heidelberg, D. Wu, M. Wu, N. Ward, M. J. Beanan, R. J. Dodson, R. Madupu, L. M. Brinkac, S. C. Daugherty, R. T. DeBoy, A. S. Durkin, M. Gwinn, J. F. Kolonay, S. A. Sullivan, D. H. Haft, J. Selengut, T. M. Davidsen, N. Zafar, O. White, B. Tran, C. Romero, H. A. Forberger, J. Weidman, H. Khouri, T. V Feldblyum, T. R. Utterback, S. E. Van Aken, D. R. Lovley, and C. M. Fraser, Genome of *Geobacter sulfurreducens*: metal reduction in subsurface environments, *Science*, vol. 302, no. 5652, pp. 1967–9, 2003.

[12] M. V. Coppi, C. Leang, S. J. Sandler, and D. R. Lovley, Development of a Genetic System for *Geobacter sulfurreducens*, *Appl. Environ. Microbiol.*, vol. 67, no. 7, pp. 3180–3187, 2001.

[13] I. Park and B. C. Kim, Homologous overexpression of omcZ, a gene for an outer surface *c*-type cytochrome of *Geobacter sulfurreducens* by single-step gene replacement, *Biotechnol. Lett.*, vol. 33, no. 10, pp. 2043–2048, 2011.

[14] Y. Liu, Z. Wang, J. Liu, C. Levar, M. J. Edwards, J. T. Babauta, D. W. Kennedy, Z. Shi, H. Beyenal, D. R. Bond, T. A. Clarke, J. N. Butt, D. J. Richardson, K. M. Rosso, J. M. Zachara, J. K. Fredrickson, and L. Shi, A trans-outer membrane porin-cytochrome protein complex for extracellular electron transfer by *Geobacter sulfurreducens* PCA, *Environ. Microbiol. Rep.*, vol. 6, no. 6, pp. 776–785, 2014.

[15] L. Zacharoff, C. H. Chan, and D. R. Bond, Reduction of low potential electron acceptors requires the CbcL inner membrane cytochrome of *Geobacter sulfurreducens*, *Bioelectrochemistry*, vol. 107, pp. 7–13, 2016.

[16] L. Morgado, A. P. Fernandes, J. M. Dantas, M. A. Silva, and C. A. Salgueiro, On the road to improve the bioremediation and electricity-harvesting skills of *Geobacter sulfurreducens*: functional and structural characterization of multihaem cytochromes, *Biochem. Soc. Trans.*, vol. 40, no. 6, pp. 1295–301, 2012.

[17] T. Khare, A. Esteve-Núñez, K. P. Nevin, W. Zhu, J. R. Yates, D. Lovley, and C. S. Giometti, Differential protein expression in the metal-reducing bacterium *Geobacter sulfurreducens* strain PCA grown with fumarate or ferric citrate, *Proteomics*, 2006, vol. 6, no. 2, pp. 632–640.

[18] K. P. Nevin and D. R. Lovley, Mechanisms for accessing insoluble Fe(III) oxide during dissimilatory Fe(III) reduction by Geothrix fermentans, *Appl. Environ. Microbiol.*, vol. 68, no. 5, pp. 2294–2299, 2002.

[19] G. Reguera, K. D. McCarthy, T. Mehta, J. S. Nicoll, M. T. Tuominen, and D. R. Lovley, Extracellular electron transfer via microbial nanowires, *Nature*, vol. 435, no. 7045, pp. 1098–1101, 2005.

[20] K. A. Weber, L. A. Achenbach, and J. D. Coates, Microorganisms pumping iron: anaerobic microbial iron oxidation and reduction, *Nat. Rev. Microbiol.*, vol. 4, no. 10, pp. 752–64, 2006.

[21] T. Mehta, M. V. Coppi, S. E. Childers, and D. R. Lovley, Outer membrane *c*-type cytochromes required for Fe(III) and Mn(IV) oxide reduction in *Geobacter sulfurreducens*, *Appl. Environ. Microbiol.*, vol. 71, no. 12, pp. 8634–8641, 2005.

[22] J. M. Dantas, Follow the red road of triheme cytochromes in *Geobacter sulfurreducens*, *Master Dissertation*, 2012.

[23] D. R. Lovley, Bug juice: harvesting electricity with microorganisms, *Nat. Rev. Microbiol.*, vol. 4, no. 7, pp. 497–508, 2006.

[24] M. Aklujkar, J. Krushkal, G. DiBartolo, A. Lapidus, M. L. Land, and D. R. Lovley, The genome sequence of *Geobacter metallireducens*: features of metabolism, physiology and regulation common and dissimilar to *Geobacter sulfurreducens*, *BMC Microbiol.*, vol. 9, no. 1, p. 109, 2009.

[25] J. F. Juárez, M. T. Zamarro, M. J. L. Barragá, B. Blázquez, M. Boll, K. Kuntze, J. L. García, E.

Díaz, and M. Carmona, Identification of the *Geobacter metallireducens* BamVW Two-Component System, Involved in Transcriptional Regulation of Aromatic Degradation, *Appl. Environ. Microbiol.*, vol. 76, no. 1, pp. 383–385, 2010.

[26] P. L. Tremblay, M. Aklujkar, C. Leang, K. P. Nevin, and D. Lovley, A genetic system for *Geobacter metallireducens*: Role of the flagellin and pilin in the reduction of Fe(III) oxide, *Environ. Microbiol. Rep.*, vol. 4, no. 1, pp. 82–88, 2012.

[27] B. M. Fonseca, C. M. Paquete, C. A. Salgueiro, and R. O. Louro, The role of intramolecular interactions in the functional control of multiheme cytochromes *c*, *FEBS Letters*, vol. 586, no. 5. pp. 504–509, 2012.

[28] K. D. Bewley, K. E. Ellis, M. A. Firer-Sherwood, and S. J. Elliott, Multi-heme proteins: Nature's electronic multi-purpose tool, *Biochimica et Biophysica Acta - Bioenergetics*, vol. 1827, no. 8–9. pp. 938–948, 2013.

[29] G. P. Moss, Nomenclature of tetrapyrroles, *Pure Appl. Chem.*, vol. 59, no. 6, pp. 779–832, 1987.

[30] L. Morgado, A. P. Fernandes, Y. Y. Londer, M. Bruix, and C. A. Salgueiro, One simple step in the identification of the cofactors signals, one giant leap for the solution structure determination of multiheme proteins, *Biochem. Biophys. Res. Commun.*, vol. 393, no. 3, pp. 466–470, 2010.

[31] P. R. Pokkuluri, Y. Y. Londer, N. E. C. Duke, W. C. Long, and M. Schiffer, Family of cytochrome c_7-type proteins from *Geobacter sulfurreducens*: structure of one cytochrome c_7 at 1.45 Å resolution, *Biochemistry*, vol. 43, pp. 849–859, 2004.

[32] L. Morgado, V. B. Paixão, M. Schiffer, P. R. Pokkuluri, M. Bruix, and C. A. Salgueiro, Revealing the structural origin of the redox-Bohr effect: the first solution structure of a cytochrome from *Geobacter sulfurreducens*, *Biochem. J.*, vol. 441, pp. 179–87, 2012.

[33] L. Morgado, M. Bruix, V. Orshonsky, Y. Y. Londer, N. E. C. Duke, X. Yang, P. R. Pokkuluri, M. Schiffer, and C. A. Salgueiro, Structural insights into the modulation of the redox properties of two *Geobacter sulfurreducens* homologous triheme cytochromes, *Biochim. Biophys. Acta - Bioenerg.*, vol. 1777, no. 9, pp. 1157–1165, Sep. 2008.

[34] P. R. Pokkuluri, Y. Y. Londer, X. Yang, N. E. C. Duke, J. Erickson, V. Orshonsky, G. Johnson, and M. Schiffer, Structural characterization of a family of cytochromes c_7 involved in Fe(III) respiration by *Geobacter sulfurreducens, Biochim. Biophys. Acta - Bioenerg.*, vol. 1797, pp. 222–232, 2010.

[35] G. W. Pettigrew and G. R. Moore, *Cytochromes c*. 1987.

[36] M. Pessanha, L. Morgado, R. O. Louro, Y. Y. Londer, P. R. Pokkuluri, M. Schiffer, and C. A. Salgueiro, Thermodynamic characterization of triheme cytochrome PpcA from *Geobacter sulfurreducens*: evidence for a role played in e^-/H^+ energy transduction, *Biochemistry*, vol. 45, pp. 13910–13917, 2006.

[37] L. Morgado, M. Brulx, M. Pessanha, Y. Y. Londer, and C. A. Salgueiro, Thermodynamic characterization of a triheme cytochrome family from *Geobacter sulfurreducens* reveals mechanistic And functional diversity, *Biophys. J.*, vol. 99, pp. 293–301, 2010.

[38] S. F. Altschul, W. Gish, W. Miller, E. W. Myers, and D. J. Lipman, Basic local alignment search tool, *J. Mol. Biol.*, vol. 215, pp. 403–410, 1990.

[39] D. S. Wishart, C. G. Bigam, A. Holm, R. S. Hodges, and B. D. Sykes, ^{1}H, ^{13}C and ^{15}N random coil NMR chemical shifts of the common amino acids. I. Investigations of nearest-neighbor effects, *J. Biomol. NMR*, vol. 5, no. 1, pp. 67–81, 1995.

[40] H. Kashima and J. M. Regan, Facultative nitrate reduction by electrode-respiring *Geobacter metallireducens* biofilms as a competitive reaction to electrode reduction in a bioelectrochemical system" *Environ. Sci. Technol.*, vol. 49, no. 5, pp. 3195–3202, 2015.

[41] E. Arslan, H. Schulz, R. Zufferey, P. Künzler, and L. Thöny-Meyer, Overproduction of the Bradyrhizobium japonicum c-type cytochrome subunits of the cbb3 oxidase in *Escherichia coli*, *Biochem. Biophys. Res. Commun.*, vol. 251, no. 3, pp. 744–747, 1998.

[42] E. A. Berry and B. L. Trumpower, Simultaneous determination of hemes *a*, *b*, and *c* from pyridine hemochrome spectra, *Anal. Biochem.*, vol. 161, no. 1, pp. 1–15, 1987.

[43] P. Leslie Dutton, Redox potentiometry: Determination of midpoint potentials of oxidation-reduction components of biological electron-transfer systems, *Methods Enzymol.*, vol. 54, pp. 411–435, 1978.

[44] C. A. Salgueiro, D. L. Turner, H. Santos, J. LeGall, and A. V. Xavier, Assignment of the redox potentials to the four haems in Desulfovibrio vulgaris cytochrome c_3 by 2D-NMR, *FEBS Lett.*, vol. 314, no. 2, pp. 155–158, 1992.

[45] H. Santos, J. J. Moura, I. Moura, J. LeGall, and a V Xavier, NMR studies of electron transfer mechanisms in a protein with interacting redox centres: Desulfovibrio gigas cytochrome c_3" *Eur. J. Biochem.*, vol. 141, no. 2, pp. 283–296, 1984.

[46] B. Bjellqvist, B. Basse, E. Olsen, and J. E. Celis, Reference points for comparisons of two-dimensional maps of proteins from different human cell types defined in a pH scale where isoelectric points correlate with polypeptide compositions, *Electrophoresis*, vol. 15, no. 3–4, pp. 529–539, 1994.

[47] C. A. Salgueiro, P. N. Da Costa, D. L. Turner, A. C. Messias, W. M. A. M. Van Dongen, L. M. Saraiva, and A. V. Xavier, Effect of hydrogen-bond networks in controlling reduction potentials in Desulfovibrio vulgaris (Hildenborough) cytochrome c_3 probed by site-specific mutagenesis, *Biochemistry*, vol. 40, no. 32, pp. 9709–9716, 2001.

[48] J. M. Dantas, D. M. Tomaz, L. Morgado, and C. A. Salgueiro, Functional characterization of PccH, a key cytochrome for electron transfer from electrodes to the bacterium *Geobacter sulfurreducens*, *FEBS Lett.*, vol. 587, no. 16, pp. 2662–2668, 2013.

[49] L. Morgado, I. H. Saraiva, R. O. Louro, and C. A. Salgueiro, Orientation of the axial ligands and magnetic properties of the hemes in the triheme ferricytochrome PpcA from G. sulfurreducens determined by paramagnetic NMR, *FEBS Lett.*, vol. 584, pp. 3442–3445, 2010.

[50] J. M. Dantas, I. H. Saraiva, L. Morgado, M. A. Silva, M. Schiffer, C. A. Salgueiro, and R. O. Louro, Orientation of the axial ligands and magnetic properties of the hemes in the cytochrome c_7 family from *Geobacter sulfurreducens* determined by paramagnetic NMR, *Dalt. transation*, vol. 40, pp. 12713–12718, 2011.

[51] Y. H. R. Ding, K. K. Hixson, M. A. Aklujkar, M. S. Lipton, R. D. Smith, D. R. Lovley, and T. Mester, Proteome of *Geobacter sulfurreducens* grown with Fe(III) oxide or Fe(III) citrate as the electron acceptor, *Biochim. Biophys. Acta - Proteins Proteomics*, vol. 1784, no. 12, pp. 1935–1941, 2008.

[52] J. R. Lloyd, C. Leang, A. L. Hodges Myerson, M. V Coppi, S. Cuifo, B. Methe, S. J. Sandler, and D. R. Lovley, Biochemical and genetic characterization of PpcA, a periplasmic *c*-type cytochrome in *Geobacter sulfurreducens*" *Biochem. J.*, vol. 369, pp. 153–161, 2003.

[53] E. S. Shelobolina, M. V Coppi, A. a Korenevsky, L. N. DiDonato, S. A. Sullivan, H. Konishi, H. Xu, C. Leang, J. E. Butler, B.-C. Kim, and D. R. Lovley, Importance of *c*-type cytochromes for U(VI) reduction by *Geobacter sulfurreducens*, *BMC Microbiol.*, vol. 7, no. Vi, p. 16, 2007.

[54] J. M. Dantas, L. Morgado, T. Catarino, O. Kokhan, P. Raj Pokkuluri, and C. A. Salgueiro, Evidence for interaction between the triheme cytochrome PpcA from *Geobacter sulfurreducens* and anthrahydroquinone-2,6-disulfonate, an analog of the redox active components of humic substances, *Biochim. Biophys. Acta - Bioenerg.*, vol. 1837, pp. 750–760, 2014.

[55] B. Thamdrup, Bacterial manganese and iron reduction in aquatic sediments, in *Advances in Microbial Ecology*, vol. 16, 2000, pp. 41–84.

[56] L. Morgado, I. H. Saraiva, R. O. Louro, and C. A. Salgueiro, Orientation of the axial ligands and magnetic properties of the hemes in the triheme ferricytochrome PpcA from *G. sulfurreducens* determined by paramagnetic NMR, *FEBS Lett.*, vol. 584, no. 15, pp. 3442–3445, 2010.

Appendix 1. Molecular weight marker (Protein plus Protein™ Dual Xtra Standards, Bio-Rad) used in the different electrophoresis performed throughout this work.

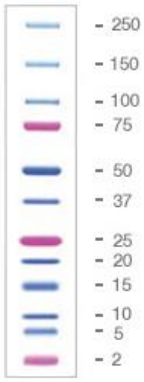

Appendix 2. Deduction of the equation used to fit the variation of the experimental reduced fraction with to solution potential in the redox titrations followed by UV-visible spectroscopy

As previously stated, a triheme cytochrome has different microstates that can be grouped into four macroscopic oxidation stages that are connected by three redox steps of one electron each (Figure 5). The different oxidation stages are related by three one-electron transfer equilibria as depicted in the scheme below

$$P_0 \underset{E_1^0}{\overset{1e^-}{\rightleftharpoons}} P_1 \underset{E_2^0}{\overset{1e^-}{\rightleftharpoons}} P_2 \underset{E_3^0}{\overset{1e^-}{\rightleftharpoons}} P_3$$

Accordingly to this scheme three Nernst equations can be defined:

$$E = E_1^0 + \frac{RT}{F} ln \frac{P_1}{P_0}$$

$$E = E_2^0 + \frac{RT}{F} ln \frac{P_2}{P_1}$$

$$E = E_3^0 + \frac{RT}{F} ln \frac{P_3}{P_2}$$

where E, corresponds to the experimental measured potential and E_1^0, E_2^0 and E_3^0 to the standard potential for each oxidation step; F represents the Faraday constant; T represents the temperature in Kelvin; and R, the gas constant. P_0, P_1, P_2 and P_3 macroscopic population in oxidation stages 0, 1, 2 and 3, respectively.

$$E = E_1^0 + \frac{RT}{F} ln \frac{P_1}{P_0} \Leftrightarrow P_1 = P_0 e^{(E - E_1^0)\frac{F}{RT}}$$

$$E = E_2^0 + \frac{RT}{F} ln \frac{P_2}{P_1} \Leftrightarrow P_2 = P_0 e^{(2E - E_1^0 - E_2^0)\frac{F}{RT}}$$

$$E = E_4^0 + \frac{RT}{F} ln \frac{P_3}{P_2} \Leftrightarrow P_3 = P_0 e^{(3E - E_1^0 - E_2^0 - E_3^0)\frac{F}{RT}}$$

Each macroscopic population can be expressed as a function of the solution potential (E) and macroscopic redox potential (E_1^0, E_2^0 and E_3^0) as follow:

$$Reduced\ fraction = \frac{3P_0 + 2P_1 + P_2}{3(P_1 + P_2 + P_3)} \Leftrightarrow$$

$$Reduced\ Fraction = \frac{3 + 2e^{\left[(E - E_1^0) \times \frac{F}{RT}\right]} + e^{\left[(2E - E_1^0 - E_3^0) \times \frac{F}{RT}\right]}}{3 \times \left(1 + e^{\left[(E - E_1^0) \times \frac{F}{RT}\right]} + e^{\left[(2E - E_1^0 - E_3^0) \times \frac{F}{RT}\right]} + e^{\left[(3E - E_1^0 - E_3^0 - E_4^0) \times \frac{F}{RT}\right]}\right)}$$

Appendix 3. Amino acid structures and designations.

Small

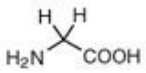

Glycine (Gly, G)
MW: 57.05

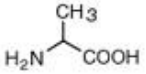

Alanine (Ala, A)
MW: 71.09

Nucleophilic

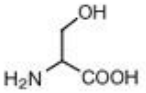

Serine (Ser, S)
MW: 87.08, pK_a ~ 16

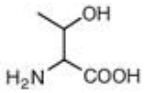

Threonine (Thr, T)
MW: 101.11, pK_a ~ 16

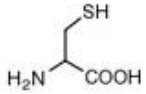

Cysteine (Cys, C)
MW: 103.15, pK_a = 8.35

Hydrophobic

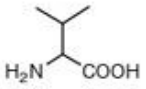

Valine (Val, V)
MW: 99.14

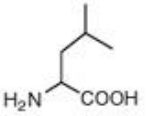

Leucine (Leu, L)
MW: 113.16

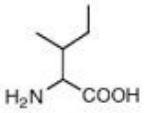

Isoleucine (Ile, I)
MW: 113.16

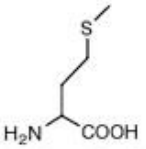

Methionine (Met, M)
MW: 131.19

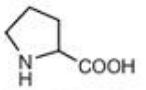

Proline (Pro, P)
MW: 97.12

Aromatic

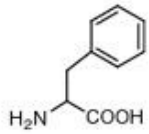

Phenylalanine (Phe, F)
MW: 147.18

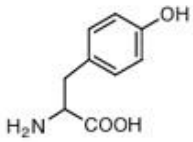

Tyrosine (Tyr, Y)
MW: 163.18

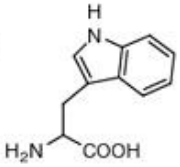

Tryptophan (Trp, W)
MW: 186.21

Acidic

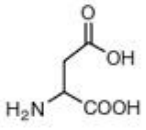

Aspartic Acid (Asp, D)
MW: 115.09, pK_a = 3.9

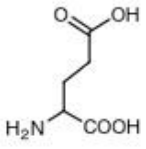

Glutamic Acid (Glu, E)
MW: 129.12, pK_a = 4.07

Amide

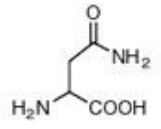

Asparagine (Asn, N)
MW: 114.11

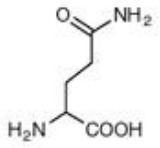

Glutamine (Gln, Q)
MW: 128.14

Basic

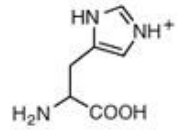

Histidine (His, H)
MW: 137.14, pK_a = 6.04

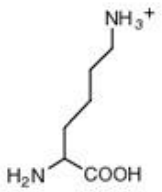

Lysine (Lys, K)
MW: 128.17, pK_a = 10.79

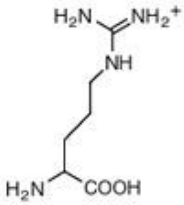

Arginine (Arg, R)
MW: 156.19, pK_a = 12.48